THE EMERGENCE OF LIQUID MIXING FROM SPINNING MAGNETIC NANOPARTICLES IN ROTATING MAGNETIC FIELDS

Visualisation and characterisation towards a better understanding of the underlying phenomena

Mémoire

Olivier Gravel

Maîtrise en génie chimique
Maître ès sciences (M. Sc.)

Québec, Canada

Résumé:

Ce travail vise à approfondir l'utilisation de nanoparticules magnétiques (NPM) en suspensions colloïdales en tant qu'agitateurs nanométriques pouvant manipuler le mélange à l'échelle micrométrique lorsque soumis à des champs magnétiques. D'abord, les structures cohérentes émergeant de la rotation de NPM sont observées par microscopie et sont quantifiées à l'aide d'une analyse multi-résolution basée sur les transformées en ondelettes, démontrant l'effet significatif des paramètres étudiés sur la génération de structures cohérentes verticales à l'intérieur du fluide. La séparation des agitateurs nanoscopiques de la phase continue à mélanger en utilisant des émulsions de nanofluides magnétiques est ensuite évaluée en comparant le couple exercé par ces émulsions en champs magnétiques avec celui de suspensions colloïdales équivalentes. Le mélange effectif similaire indique, pour des champs magnétiques rotatifs, que le momentum développé par les NPM en rotation est en mesure de se transmettre aux gouttelettes ainsi qu'à la phase continue des émulsions.

Abstract:

The present work further explores the use of MNPs in colloidal suspensions as nano-scale devices to manipulate mixing at the micro-scale when the whole system is subject to magnetic fields. First, the coherent structures emerging from rotating MNPs are visually observed using a microscopic imaging protocol and are quantitatively analyzed with a multi-resolution wavelet transforms based technique. The results demonstrate the significant effect of nanofluid composition and magnetic field parameters on the inception of coherent vortical structures inside the fluid. Secondly, the separation of the stirring MNPs from the continuous phase by using magnetic nanofluid emulsions is evaluated by comparing the torque exerted by MNPs in emulsions with the one in equivalent colloidal suspensions under magnetic fields. The very similar effective mixing indicates, for rotating magnetic fields, that the momentum developed by spinning MNPs inside emulsion droplets is transferable not only to the droplets but also to the surrounding liquid.

Table of contents

List of tables:

List of figures:

À Muriel

« No rest is worth anything except the rest that is earned. »
- Jean Paul

Remerciements:

Tout premièrement, je tiens à remercier mon directeur de recherche, Professeur Faïçal Larachi, pour son accueil au sein de son groupe de recherche, pour son encadrement au cours de mon parcours inhabituel ainsi que pour les amples connaissances et l'expertise qui sont les siennes et qu'il a mis à ma disposition. C'est un honneur pour moi d'apprendre en tant que chercheur et d'évoluer à vos côtés. Merci aussi au Professeur Carl Duchesne pour son aide ainsi que son implication en tant que co-directeur.

Je tiens aussi à remercier profondément Dr. Pouya Hajiani de m'avoir intégré à son projet de recherche, ainsi que de m'avoir initié, éduqué et guidé à travers un sujet multidisciplinaire, complexe et souvent ardu. Il est responsable de la fondation de tous mes travaux, et je lui suis plus que reconnaissant de sa patience, sa rigueur ainsi que de son esprit calme et analytique, qui m'ont énormément influencé.

Merci aussi à mes collègues et amis pour leur support et leur aide au cours des dernières années. Dr. Amin Sarvaramini, Dr. Gnouyaro Palla Assima, Ali Faridkhou, Hadk Ahmed Cherif et Shahab Boroun, je vous remercie pour votre assistance, vos commentaires et pour le bon climat qui règne au sein du groupe de recherche.

Je remercie les techniciens du département de génie chimique de l'Université Laval, notamment Jérôme Noël, Marc Lavoie et Jean-Nicolas Ouellet pour leur aide et leur disponibilité.

Mes sincères remerciements sont aussi dirigés vers Christine Berthiaux, Nicolas Corneau-Tremblay, Vincent Gravel et Simon Gravel. Sans votre continuelle compréhension, votre support et votre aide cruciale, je n'aurais jamais pu terminer ce travail. Merci beaucoup.

Finalement, merci à Dr. Jean-François Boucher de m'avoir inspiré vers les études graduées et merci tout spécialement à mes parents, Paul Gravel et Nicole Boucher, pour leur amour et leur support inconditionnel. Je vous dois tout.

Acknowledgments:

First of all, I would like to thank my advisor, Professor Faïçal Larachi, for my acceptance into his research group, for his guidance along my unusual journey and for sharing with me his vast knowledge and expertise. It is an honour for me to learn and to grow as a researcher under your tutelage. Thanks also to Professor Carl Duchesne, for his help and his implication as my co-advisor.

Secondly, I would like to thank Dr. Pouya Hajiani for including me into his research project and for teaching and guiding me through an often complex multidisciplinary project. He is responsible for the foundation of my work in the group, and I am grateful for his patience, his rigor and for his calm and analytic mind which have had a great influence on me.

I would also like to thank my friends and colleagues for their help and support during the last few years. Dr. Amin Sarvaramini, Dr. Gnouyaro Palla Assima, Ali Faridkhou, Hadk Ahmed Cherif and Shahab Boroun, thank you for your assistance, your comments and for the god climate existing in the research group.

The help of technical staff from the chemical engineering department of Université Laval during this project is also appreciated. Jérome Noël, Marc Lavoie, and Jean-Nicolas Ouellet, thank you for your help and availability.

My sincere gratitude is also directed towards Christine Berthiaux, Nicolas Corneau-Tremblay, Vincent Gravel and Simon Gravel. Without your continual understanding, your support and your crucial help in time of need, I could never have finished this work. Thank you.

Finally, thanks to Dr. Jean-François Boucher for inspiring me and steering me toward graduate studies from a young age and a very special thanks to my dear parents, Nicole Boucher and Paul Gravel, for their love and unconditional support. I owe you everything I am. Thank you.

Foreword:

This work comprises four chapters. The first is an introduction and a literature review relevant to the project at hand. The two following chapters, for their part, represent a published article, accepted or submitted in scientific journals. The fourth and last chapter concludes by presenting this work's key contributions and opens for future works.

I am the principal author of both articles. I completed the experimental work, the analysis and the redaction under the supervision of my advisor, Professor Faïçal Larachi. My co-advisor, Professor Carl Duchesne, oversaw the mathematical analysis part of the article he participated in. A graduate student under his supervision, Julien Lauzon-Gauthier, assisted in the creation and implementation of the Matlab program required for the analysis and helped in the redaction of the image analysis section of the article. Dr. Pouya Hajiani provided the theoretical framework for the article he participated in. In both cases the article redaction was corrected and amended by my co-authors.

Publications:

Gravel, O., Lauzon-Gauthier, J., Duchesne, C. & Larachi, F. (2014) Inception of vortical coherent structures from spinning magnetic nanoparticles in rotating magnetic fields – New nanofluid microscale mixing tool. *Chemical Engineering Journal* (submitted)

Olivier, G., Pouya, H., & Faïçal, L. (2014). Magnetically induced agitation in liquid-liquid-magnetic nanoparticle emulsions: Potential for process intensification. *AIChE Journal*. 60: 1176–1181

CHAPTER I.

Introduction and scope of the project

I.1. Magnetic nanoparticles:

Since their emergence into modern science's spotlight in the early 1960's [1], magnetic nanoparticles (MNPs) have attracted a lot of interest and have found their way through diverse science and engineering applications. Concisely, MNPs in the recent years have been employed with multifarious intents in fields ranging from biotechnology [2-5], biomedicine [6-11], water treatment and purification [12-18], acoustics [1], data-storage [19], magneto-optics [20-23], microfluidic devices [24-26], and catalysis [27, 28]. These submicronic particles are generally composed of elements such as iron, nickel, cobalt and their alloys [29]. For their part, the most prevalently studied MNPs consist of magnetite (Fe_3O_4) and maghemite (Fe_2O_3) due to their relative ease of synthesis and chemical modification as well as their non-toxicity and low cost [30].

I.2. Magnetic properties:

Ferromagnetism (here including ferrimagnetism), the strongest type of magnetism defining any material with the ability to exhibit spontaneous magnetization, is the one at play in MNPs. However, this foremost property of the magnetic materials composing MNPs is governed by the effects of size and chemical composition of the nanoparticles. To make sense of the impact of MNP size on their magnetic properties, the concept of magnetic domains has to be introduced and thoroughly analyzed. Concisely, a fragment of ferromagnetic material can be thought of as divided in very small regions called magnetic domains [31] within which the spins are aligned. This happens spontaneously because the exchange interaction, a quantum mechanical effect between identical particles, is a short-range force, and hence over the distance of many atoms the propensity of magnetic dipoles to reduce their energy by orienting in opposite directions prevails [29].This will give rise to a material split into several domains pointing in different directions separated by domain walls, or transition zones of finite thickness in which the magnetization direction of the dipoles gradually changes from one domain's direction to the other [32].

It is this domain structure that determines the magnetic behaviour size dependence of a ferromagnetic material [33]. More precisely, the most important finite-size effects in nanoparticles are the single domain limit and the superparamagnetic limit [33]. On the larger end of the spectrum, the MNPs are understandably multi-domain, but for each type of MNP exists a particle diameter at which a transition from multi-domain to single-domain occurs. This diameter is referred to as the critical diameter (D_{sd}), as seen in figure I.1.

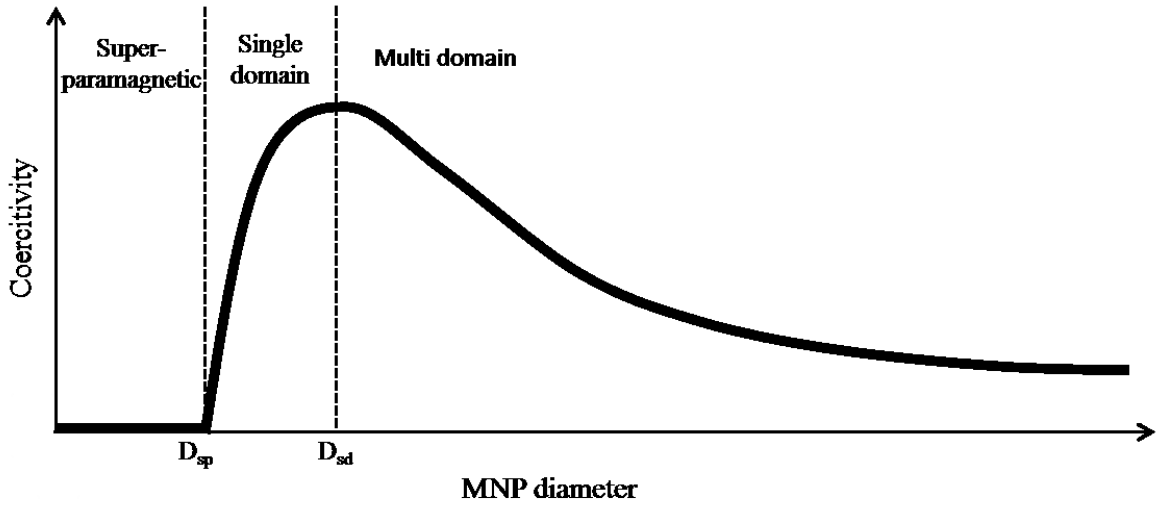

Figure I.1: Effect of particle size on the coercivity of typical MNPs

As previously stated, the multi-domain configuration results from the balance between the magnetostatic energy of the particle and domain wall energy and therefore, with a reduction in particle size, a threshold can be reached where all the magnetic spins inside a particle can exist in a single magnetic domain since below this threshold it costs more energy to create a domain wall than to support the magnetostatic energy of the single-domain state [32]. With a further reduction in particle size, a second critical diameter (denoted as D_{sp}), can be reached and is linked with the apparition of superparamagnetism, where magnetization can randomly flip direction under the influence of temperature. More precisely, at this point the thermal fluctuations at room temperature, or Brownian perturbation sources, are strong enough to spontaneously demagnetize a previously saturated assembly of dipolar interactions and hence the nanoparticles have zero coercivity (as shown in figure I.1) and no hysteresis [34]. Therefore, superparamagnetic nanoparticles are in a non-magnetic state in the absence of an applied field, become magnetic when submitted to an external magnet

and revert to their non-magnetic state when it is removed. This feature allows for the avoidance of any MNP active behavior in the absence of a magnetic field when required, thus making superparamagnetic nanoparticles the most attractive for versatile applications. Withal, it is also important to consider that the two critical diameters previously introduced are strongly dependent on the chemical composition of the MNPs. This dependency is shown in figure I.2 with the comparison of critical diameters for various MNPs with different chemical compositions. The difference among their transition diameters are obvious and in some cases outstanding. As can be seen, in coherence with their popularity status, magnetite and maghemite MNPs have some of the largest known D_{sp}, providing a vaster synthesis and application range within the confines of superparamagnetism.

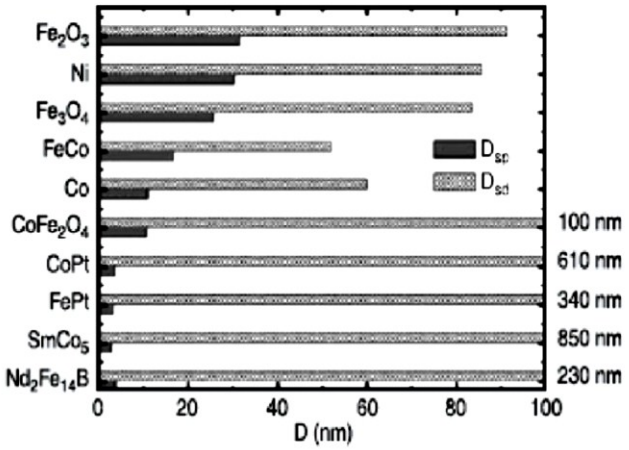

Figure I.2: Single-domain size (D_{sd}) and superparamagnetic transition size (D_{sp}) of selected ferromagnetic materials [30]

I.3. Magnetic nanoparticle synthesis:

As mentioned, iron oxides MNPs, due to their various qualities, have been the most popular and thoroughly studied nanoparticles. Consequently, various synthesis protocols and modification methods have been devised and tested in different conditions and for a wide range of purposes [35]. The most commonly encountered ones are hydrothermal synthesis, co-precipitation, chemical vapour deposition, electro-deposition and thermal deposition. Out of these, the co-precipitation method has been the most popular, as it is a facile and convenient way to synthesize iron oxide MNPs from aqueous salt solutions without using hazardous materials or the need of high temperature processing. The only drawback of this

route is that the controlling the particle size distribution is not completely practicable [35]. Further surface modification, for its part, can be implemented by surface modification via covalent or non-covalent functionalization of the iron oxide MNPs with organic (i.e. polymers, acids) and inorganic (i.e. silica, carbon) species [33].

I.4. Magnetic field response:

The application of external magnetic fields to magnetic nanofluids unsurprisingly has notable effects on fluid behavior and properties. To adequately understand the provenance of these effects, one of the first factors to consider is that two types of MNPs can be distinguished when it comes to the freedom of rotation of the magnetic moment vector inside their solid crystal structures. First, there are the rigid dipoles magnetic nanoparticles (rdMNPs) [36] in which the strong anisotropic energy locks the magnetic moment inside the solid crystal. Oppositely, in the second type of particles, antagonistically called soft dipoles magnetic nanoparticles (sdMNPs), the magnetic moment can freely rotate inside the solid crystal structure in response to thermal agitation perturbations, thus exhibiting superparamagnetism [37]. Accordingly, these two types of particles react differently to the torque exerted by an applied magnetic field on their magnetic dipole moments, which acts to align them in the field direction [5]. For rdMNPs, since the magnetic moment is locked inside the solid crystal, this torque is also felt through the solid body and has the potential to cause an "asynchronous" angular motion with respect to the surrounding fluid. This bodily torque is however not required for sdMNPs in order to obtain an alignment of the magnetic moments. In the case where a sufficiently strong stationary magnetic field is applied, rdMNP spin can even be blocked regardless of flow vorticity while in the same case sdMNP spin would follow the surrounding flow vorticity.

A more comprehensive theoretical and mathematical description of the relevant framework for ferrofluid applications in chemical engineering can be found in a review by Hajiani and Larachi [38] but to summarize, magnetization, or the macroscopic magnetic response of a material, can be described for magnetic nanofluids in a magnetohydrostatic context by Langevin's magnetization equation [5] on the following page:

$$M_0 = M_s(\alpha)\frac{H}{H'},\ L(\alpha) = coth(\alpha) - \alpha^{-1},\ \alpha = \frac{\mu_0 m_p H}{k_B T},\ H = |H| \quad (1)$$

Where M_0 is the equilibrium magnetization; L is the Langevin magnetization function operator; m_p is the magnetic dipole moment of one single MNP; M_s is the saturation magnetization occurring when all the MNP magnetic moments are aligned with the external magnetic field H; H' is the fluctuating component of magnetic field caused by turbulence; α is the dimensionless Langevin module; μ_0 is the vacuum permeability; k_B is the Boltzmann constant and T is the temperature.

When a magnetic field is applied to a magnetic nanofluid such that a saturation magnetization is achieved, once the field is disabled, this magnetization will decay following [37]:

$$M = M_s e^{-t/\tau} \quad (2)$$

Where τ_m is the observational time scale of the experiment and τ is a relaxation time constant. While for $\tau_m << \tau$ the instantaneous magnetization remains stable near M_s over τ_m, for $\tau_m >> \tau$, it decays to zero as time progresses due to the randomizing effect of thermal agitation on the magnetic moments [37]. This thermal agitation randomizes the magnetic moments following different mechanisms for rdMNPs and sdMNPs. rdMNPs rotate bodily as a result of Brownian collisions and are characterized by a time constant τ_B [5] from the following equation:

$$\tau_B = 3V_h\mu/k_B T \quad (3)$$

Where V_h is the MNP hydrodynamic volume, μ is the dynamic viscosity, k_B is the Boltzmann constant and T is the temperature. For sdMNPs, since the magnetic moment can freely rotate inside the solid crystal structure, they do not require a bodily rotation, and so their Néelian relaxation time constant can be found using the following Néel-Arrhénius equation:

$$\tau_N = \tau_0 \exp\left(\frac{KV_p}{k_B T}\right) \quad (4)$$

Where τ_0 is the attempt period characteristic of the material (usually around 10^{-9} to 10^{-10} second), KV is the energy barrier defined by the MNP anisotropic energy density (K) and its core volume (V_p), k_B is the Boltzmann constant and T is the temperature. For instances when both types of MNPs are present in a nanofluid, as is sometimes the case in commercial ferrofluids, Martsenyuk et al. [6] proposed to use an effective relaxation time constant defined as a harmonic mean between τ_B or τ_N [39], reflecting more weight by the smaller of the two relaxation times:

$$\tau = \frac{\tau_N \tau_B}{\tau_N + \tau_B} \tag{5}$$

In practice, different circumstances of a dynamic nature can arise when the magnetization vector cannot catch up instantaneously with the equilibrium magnetization vector. A relevant example would be in time-varying magnetic fields such as rotating or oscillating magnetic fields. Indeed, in the case of MNPs in magnetic nanofluids under rotating magnetic fields (RMFs), the magnetization vector lags behind the magnetic field vector due to the relaxation time and in oscillating magnetic fields (OMFs), despite collinearity between the magnetization vector and the magnetic field vector, relaxation is also a factor because of a distribution of misalignments in magnetic dipoles. In RMFs, by trying to catch up to the ever-changing magnetic field vector, the exerted angular torque will cause the MNPs to rotate with respect to the surrounding liquid. For rdMNPs, this angular magnetic torque felt bodily is associated with a momentum transferable to the adjacent liquid phase [40], and thus can impart an angular motion to the liquid. As long as the magnetic nanofluids are sufficiently diluted so that the mutual magnetic interactions among MNPs are negligible [41,42], the seeded MNPs can be considered as independent nanostirrers generating mixing effects their individual selves. A graphic representation of this phenomenon from previous works [43] can be found in figure I.3.

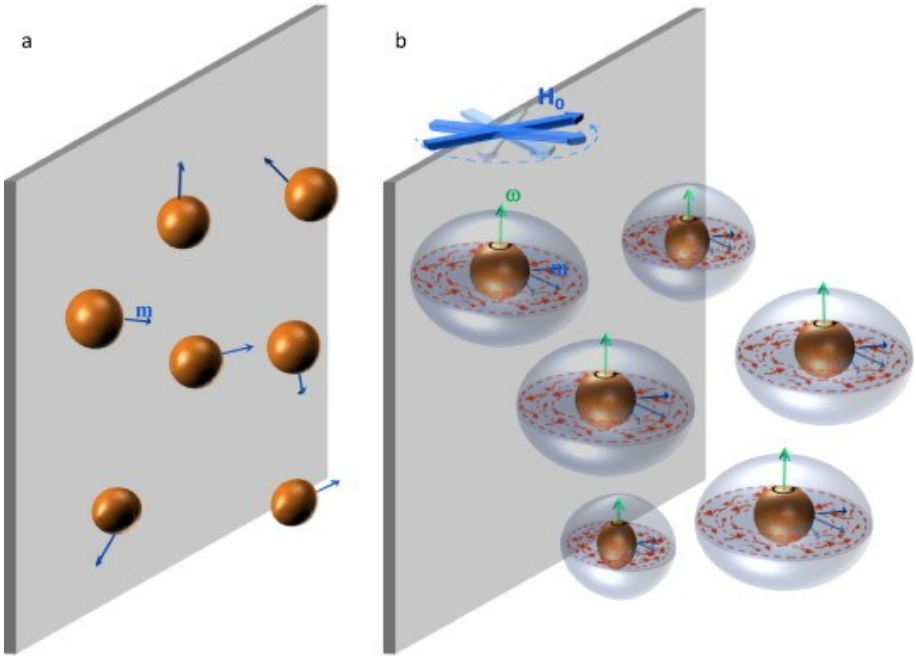

Figure I.3: Schematic diagram of MNPs spin in hydrostatic conditions with and without uniform RMF (a) in absence of magnetic field, MNPs gyration and translation is solely due to Brownian thermal agitation; MNP time-average spin vector (ω) is equal to zero since MNP magnetic moments (m) are randomized in all directions and (b) in presence of uniform RMF (H_0), MNP spin vector (ω) turns normal to H_0 and hence lateral mixing occurs in all directions. [43]

I.5. Magnetic nanofluid induced mixing:

Most of the foundation for the study of the response of magnetic nanofluids to time-varying magnetic fields with focus of mixing generation originates from the various studies on magnetoviscosity initiated by Rosensweig et al. [44] and McTague [45] and for which the theoretical framework was established by Shliomis [46] and Mozorov [36]. From the theoretical framework, Bacri et al. [47] and Zeuner et al. [40] then experimentally explored the way in which the anisotropic apparent viscosity appearing under magnetic fields, stemming from the rdMNPs being pinned by the magnetic field forcing them to spin asynchronously relative to the contiguous fluid, leads ferrofluids to exert shear stress on the wall with respect to the magnetic field parameters in OMFs [5]. In these works, both positive and negative rotational magnetoviscosity were registered, emanating from the energy transfers from the OMF to the fluid flow via rdMNP kinetic energy. However, under OMFs, both the magnetic field and the magnetization vector pass via a zero point

during the oscillation cycle, resulting in a strong dependence of the rotational behavior of rdMNPs on fluid vorticity time scale (τ_h), OMF oscillation time scale (τ_{AC}) and the Brownian relaxation time constant (τ_B) [38]. If the magnetic field oscillation time scale is small enough, the thermal agitation mechanism is able to destroy the magnetization vector by shuffling MNPs during the off-field moment in the middle of the oscillation cycle, preventing a true continual rotation. This fact led to experimentations with RMFs where neither magnetic field nor magnetization vector pass via zero point during a cycle and thus where synchronized rotation of rdMNPs is attainable even in low field frequencies. Marcus Zahn's research group at MIT investigated this phenomenon by conducting torque measurement experiments on ferrofluid submitted to RMFs (Rosenthal et al. [48], Rinaldi et al. [41], and He et al. [42]). Along with the following works from Sànchez and Rinaldi [49], they showed that in the negative magnetoviscosity regions, the particles in a co-rotating magnetic field will rotate faster than in an oscillating magnetic field, and that the flow due to co-rotating particles is strong enough to obtain a negative effective viscosity for dilute suspensions.

With these results in mind, more recently, MNPs were studied to enhance transport operations beyond what can be accomplished in the classical paradigm. In an approach first proposed by Suresh and Bhalerao [50], the effects of MNPs on carbon dioxide absorption using an OMF to enhance gas-liquid interfacial mass transfer in a wetted-wall falling-film column and a bubble. Olle et al. [51] subsequently measured a diminution of surface tension in these conditions, indicating that MNP are enough small to protrude through, and populate, the liquid diffusional boundary layer. Consequently, MNPs stimulated by an external magnetic emulate microscale stirrers in the liquid diffusional boundary layer and doing so, decrease interfacial mass transfer resistance.

With the table then set for the examination of genuine nanomixing from the action of MNPs under magnetic fields, Hajiani and Larachi in the last five years have investigated the phenomenon under different scenarios. In the first instance [52], following the results from Olle et al. [51], the mixing and hindrance effects of MNPs under magnetic fields were incorporated into a gas-liquid mass transfer system in Taylor flow regime. In this scenario where the hydrodynamic shear rate around Taylor bubbles is substantially stronger than

that of low Reynolds number single phase flow in capillaries, the mixing effect of spinning MNPs and mass transfer enhancement in lubricating file were found to be marginal. The gas-liquid mass transfer rate was also found to decrease up to 10 percent by magnetically locked MNPs under a static magnetic field (SMF).

Secondly, it was demonstrated that nanomixing in a controlled direction can give rise to lateral mixing in presence of low Reynolds convective flows in capillary [53]. By investigating the axial dispersion in magnetic nanofluids flowing through a Taylor capillary cell under moderate strength and low frequency transverse RMFs, the results point to spinning MNPs generating nano-sized vortices that objectively enhance lateral mixing beyond the capability of molecular diffusion. In these experiments, the active magnetic torque is able to overcome the hydrodynamic torque which tends to gyrate MNPs perpendicularly to the MNP spin plane. During a systematic study of the system parameters, a plateauing effect was observed with respect to MNP concentration and field frequency. This effect was explained and attributed to the size of mixed spheroid zones around single MNPs. Furthermore, using the RTD data, the laminar velocity profile was reconstructed in the presence and absence of magnetic field. Under transverse RMF, the slight shear-thinning behaviour of the nanofluid flattened the originally parabolic velocity profile toward plug flow like profile. A subsequent study bringing attention to the effects of different magnetic field scenarios on the axial dispersion variation and laminar velocity profile found that OMFs did not have significant effect on lateral mixing in capillary. Axial static magnetic fields also acted in a way coherent to them locking the MNPs and making them resist rotation with surrounding fluid vorticity. Finally, a shear-thickening behavior was detected under axial SMFs with the reconstructed laminar velocity profile protruding from no-field parabolic profile.

Most importantly for the present body of work, the effect of a magnetic nanofluid on self-diffusion in stagnant liquid was also examined [43]. Conductimetric tracer impulse injections were carried out for the determination of the liquid apparent self-diffusivity in a stagnant liquid enclosed in a diffusion cell for varying conditions of magnetic intensity and frequency, and nanoparticle volume fraction. To assess the extent of magnetic stimulation, a diffusion enhancement factor was defined as the ratio of apparent self-diffusivity under

RMF to that in absence of magnetic field (D_0) under otherwise similar flow rate conditions. The variations of D/D_0 as a function of the studied parameters are shown in figure I.4.

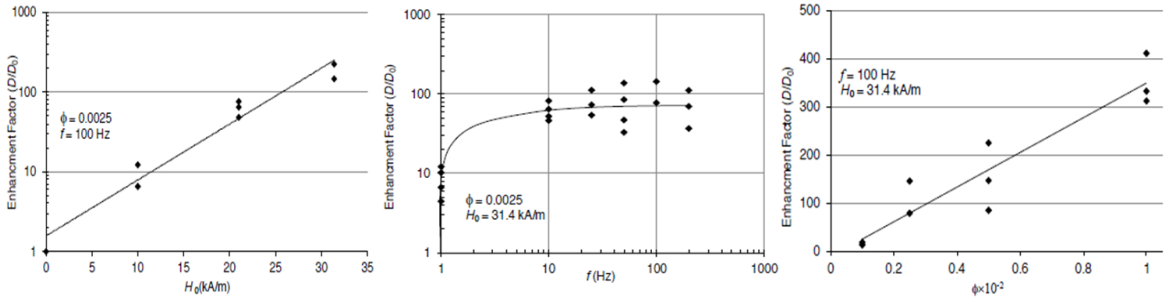

Figure I.4: Diffusion enhancement factor under RMF: Effect of (a) magnetic field strength; (b) magnetic field frequency; (c) MNP concentration. D_0 is liquid self-diffusion coefficient without magnetic field [43]

From these results, it is clear that magnetically-excited spinning MNPs generate nanomixing in capillaries as they significantly enhance self-diffusivity in every case. This in turn supports the assumption that RMFs deliver electromagnetic energy into the liquid phase through the spinning MNPs. The tentative explanation speculates that a nano-convective spheroid zone forms around each MNP in which the mixing mechanism is enhanced by particle motion. Thus, for the distance between two neighboring MNPs, the length scale within which molecular diffusion is the dominant transport mechanism decreases and the mass transfer rate significantly increases. The enhancement factor can be heightened or lowered by tweaking to magnetic field amplitude, frequency and MNP concentration.

I.6. Scope of the project :

Following the work Hajiani and Larachi in the last few years [28, 43, 52-56], which provided experimental data on transport phenomenon in the presence of magnetically excited MNPs suspended in liquid for fluid-fluid enhancement processes relevant to chemical reaction engineering, the purpose of this research is twofold.

First of all, since the previously presented body of work on MNP induced mixing has studied the phenomenon using methods and measurements that could be qualified as indirect with regards to mixing behavior, such as diffusion or axial dispersion coefficients, a protocol allowing direct visualisation of the mixing action inside usually too opaque magnetic nanofluids while they are subjected to different magnetic fields is devised and implemented. Doing so provides the first known images and videos of the coherent vortical structures generated by spinning MNPs in rotating magnetic fields and their visual characteristics with respect to the magnetic nanofluid composition (magnetic core volume fraction, MNP size) and to the magnetic field parameters (intensity, frequency and type). To quantifiably support the interpretations derived from the visual observations, a multi-resolution orthogonal wavelet analysis coupled with a particle detection and measurement algorithm is developed and applied. The impacts of the different factors as well as the implications of the uncovered information are then thoroughly discussed.

Secondly, in pursuit of the development of a versatile rotating MNP based mixing technology, there is a need to address the potential applications in which direct contact between surfactant-stabilized MNPs and the continuous liquid phase to be mixed would be proscribed. One could think of the applications where chemical interations between stabilizing surfactants or MNPs and desirable chemicals could impede transformation. For these cases, the use of oil-based magnetic nanofluid emulsions in aqueous phase is investigated. The potential mixing energy transferred to the continuous phase is assessed using torque measurements inside the emulsions when submitted to different magnetic fields and the comparison is made with colloidal aqueous suspensions of the same MNPs of equivalent magnetic content.

I.7. References :

[1] Rosensweig, R. E. (2013). Ferrohydrodynamics. Courier Dover Publications.

[2] Gupta, A. K., & Gupta, M. (2005). Synthesis and surface engineering of iron oxide nanoparticles for biomedical applications. *Biomaterials*, 26(18), 3995-4021.

[3] Liu, C. J., Lien, K. Y., Weng, C. Y., Shin, J. W., Chang, T. Y., & Lee, G. B. (2009). Magnetic-bead-based microfluidic system for ribonucleic acid extraction and reverse transcription processes. *Biomedical microdevices*, 11(2), 339-350.

[4] Hatch, G. P., & Stelter, R. E. (2001). Magnetic design considerations for devices and particles used for biological high-gradient magnetic separation (HGMS) systems. *Journal of Magnetism and Magnetic Materials*, 225(1), 262-276.

[5] Chung, S. H., Hoffmann, A., Bader, S. D., Liu, C., Kay, B., Makowski, L., & Chen, L. (2004). Biological sensors based on Brownian relaxation of magnetic nanoparticles. *Applied physics letters*, 85(14), 2971-2973.

[6] Majewski, P., & Thierry, B. (2007). Functionalized magnetite nanoparticles—synthesis, properties, and bio-applications. *Critical Reviews in Solid State and Materials Sciences*, 32(3-4), 203-215.

[7] Ito, A., Shinkai, M., Honda, H., & Kobayashi, T. (2005). Medical application of functionalized magnetic nanoparticles. *Journal of bioscience and bioengineering*, 100(1), 1-11.

[8] Neuberger, T., Schöpf, B., Hofmann, H., Hofmann, M., & von Rechenberg, B. (2005). Superparamagnetic nanoparticles for biomedical applications: possibilities and limitations of a new drug delivery system. *Journal of Magnetism and Magnetic Materials*, 293(1), 483-496.

[9] Kopelman, R., Lee Koo, Y. E., Philbert, M., Moffat, B. A., Ramachandra Reddy, G., McConville, P., ... & Ross, B. D. (2005). Multifunctional nanoparticle platforms for in vivo MRI enhancement and photodynamic therapy of a rat brain cancer. *Journal of Magnetism and Magnetic Materials*, 293(1), 404-410.

[10] Kalambur, V. S., Han, B., Hammer, B. E., Shield, T. W., & Bischof, J. C. (2005). In vitro characterization of movement, heating and visualization of magnetic nanoparticles for biomedical applications. *Nanotechnology*, 16(8), 1221.

[11] Jordan, A., Scholz, R., Wust, P., Fähling, H., & Felix, R. (1999). Magnetic fluid hyperthermia (MFH): Cancer treatment with AC magnetic field induced excitation of biocompatible superparamagnetic nanoparticles. *Journal of Magnetism and Magnetic Materials*, 201(1), 413-419.

[12] Bromberg, L., & Hatton, T. A. (2007). Decomposition of toxic environmental contaminants by recyclable catalytic, superparamagnetic nanoparticles. *Industrial & engineering chemistry research*, 46(10), 3296-3303.

[13] Bromberg, L., & Hatton, T. A. (2005). Nerve agent destruction by recyclable catalytic magnetic nanoparticles. *Industrial & engineering chemistry research*, 44(21), 7991-7998.

[14] Zhao, X., Shi, Y., Wang, T., Cai, Y., & Jiang, G. (2008). Preparation of silica-magnetite nanoparticle mixed hemimicelle sorbents for extraction of several typical phenolic compounds from environmental water samples. *Journal of Chromatography A*, 1188(2), 140-147.

[15] Huang, S. H., & Chen, D. H. (2009). Rapid removal of heavy metal cations and anions from aqueous solutions by an amino-functionalized magnetic nano-adsorbent. *Journal of Hazardous Materials*, 163(1), 174-179.

[16] Li, H., Li, Z., Liu, T., Xiao, X., Peng, Z., & Deng, L. (2008). A novel technology for biosorption and recovery hexavalent chromium in wastewater by bio-functional magnetic beads. *Bioresource technology*, 99(14), 6271-6279.

[17] Rocher, V., Siaugue, J. M., Cabuil, V., & Bee, A. (2008). Removal of organic dyes by magnetic alginate beads. *Water research*, 42(4), 1290-1298.

[18] Yantasee, W., Warner, C. L., Sangvanich, T., Addleman, R. S., Carter, T. G., Wiacek, R. J., Fryxell, G.E., Timchalk, C. & Warner, M. G. (2007). Removal of heavy metals from aqueous systems with thiol functionalized superparamagnetic nanoparticles. *Environmental science & technology*, 41(14), 5114-5119.

[19] Frolov, G. I. (2001). Film carriers for super-high-density magnetic storage. *Technical Physics*, 46(12), 1537-1544.

[20] Hasmonay, E., Depeyrot, J., Sousa, M. H., Tourinho, F. A., Bacri, J. C., Perzynski, R., ... & Rosenman, I. (2000). Magnetic and optical properties of ionic ferrofluids based on nickel ferrite nanoparticles. *Journal of Applied Physics*, 88(11), 6628-6635.

[21] Hasmonay, E., Depeyrot, J., Sousa, M. H., Tourinho, F. A., Bacri, J. C., & Perzynski, R. (1999). Optical properties of nickel ferrite ferrofluids. *Journal of magnetism and magnetic materials*, 201(1), 195-199.

[22] Hasmonay, E., Dubois, E., Neveu, S., Bacri, J. C., & Perzynski, R. (2001). Alternating magneto-birefringence of ionic ferrofluids in crossed fields. *The European Physical Journal B-Condensed Matter and Complex Systems*, 21(1), 19-29.

[23] Martin, J. E., Hill, K. M., & Tigges, C. P. (1999). Magnetic-field-induced optical transmittance in colloidal suspensions. *Physical Review E*, 59(5), 5676.

[24] Ahn, C. H., Allen, M. G., Trimmer, W., Jun, Y. N., & Erramilli, S. (1996). A fully integrated micromachined magnetic particle separator. *Journal of Microelectromechanical Systems*, 5(3), 151-158.

[25] Pamme, N., & Manz, A. (2004). On-chip free-flow magnetophoresis: continuous flow separation of magnetic particles and agglomerates. *Analytical Chemistry*, 76(24), 7250-7256.

[26] Pamme, N. (2006). Magnetism and microfluidics. *Lab on a Chip*, 6(1), 24-38.

[27] Teunissen, W., de Groot, F. M., Geus, J., Stephan, O., Tence, M., & Colliex, C. (2001). The structure of carbon encapsulated NiFe nanoparticles. *Journal of Catalysis*, 204(1), 169-174.

[28] Hu, A., Yee, G. T., & Lin, W. (2005). Magnetically recoverable chiral catalysts immobilized on magnetite nanoparticles for asymmetric hydrogenation of aromatic ketones. *Journal of the American Chemical Society*, 127(36), 12486-12487.

[29] Gubin, S. P. (Ed.). (2009). Magnetic nanoparticles. John Wiley & Sons.

[30] Poudyal, N., & Liu, J. P. (2013). Advances in nanostructured permanent magnets research. *Journal of Physics D: Applied Physics*, 46(4), 043001.

[31] Feynman, R. P., Leighton, R. B., & Sands, M. (2013). The Feynman Lectures on Physics, Desktop Edition Volume I (Vol. 1). Basic Books.

[32] Aharoni, A. (2000). Introduction to the Theory of Ferromagnetism (Vol. 109). Oxford University Press.

[33] Lu, A. H., Salabas, E. E., & Schüth, F. (2007). Magnetic nanoparticles: synthesis, protection, functionalization, and application. *Angewandte Chemie International Edition*, 46(8), 1222-1244.

[34] Krishnan, K. M. (2010). Biomedical nanomagnetics: a spin through possibilities in imaging, diagnostics, and therapy. *IEEE Transactions on magnetics*, 46(7), 2523-2558.

[35] Laurent, S., Forge, D., Port, M., Roch, A., Robic, C., Vander Elst, L., & Muller, R. N. (2008). Magnetic iron oxide nanoparticles: synthesis, stabilization, vectorization, physicochemical characterizations, and biological applications. *Chemical reviews*, 108(6), 2064-2110.

[36] Morozov, K., Shliomis, M., & Zahn, M. (2006). Magnetoviscosity in suspensions of grains with finite magnetic anisotropy. *Physical Review E*, 73(6), 066312.

[37] Morrish, A. H. (2001). The physical principles of magnetism. *The Physical Principles of Magnetism*, by Allan H. Morrish, pp. 696. ISBN 0-7803-6029-X. Wiley-VCH, January 2001, 1.

[38] Hajiani, P., & Larachi, F. (2009). Ferrofluid applications in chemical engineering. Int. *Rev. Chem. Eng*, 2, 221-237.

[39] Odenbach, S., & Thurm, S. (2002). Magnetoviscous effects in ferrofluids (pp. 185-201). Springer Berlin Heidelberg.

[40] Zeuner, A., Richter, R., & Rehberg, I. (1998). Experiments on negative and positive magnetoviscosity in an alternating magnetic field. *Physical Review E*, 58(5), 6287-6293.

[41] Rinaldi, C., Gutman, F., He, X., Rosenthal, A. D., & Zahn, M. (2005). Torque measurements on ferrofluid cylinders in rotating magnetic fields. *Journal of magnetism and magnetic materials*, 289, 307-310.

[42] He, X., Elborai, S., Kim, D., Lee, S. H., & Zahn, M. (2005). Effective magnetoviscosity of planar-Couette magnetic fluid flow. *Journal of applied physics*, 97(10), 10Q302-10Q302.

[43] Hajiani, P., & Larachi, F. (2013). Giant effective liquid-self diffusion in stagnant liquids by magnetic nanomixing. *Chemical Engineering and Processing: Process Intensification*, 71, 77-82.

[44] Rosensweig, R. E., Kaiser, R., & Miskolczy, G. (1969). Viscosity of magnetic fluid in a magnetic field. *Journal of Colloid and Interface Science*, 29(4), 680-686.

[45] McTague, J. P. (2003). Magnetoviscosity of magnetic colloids. *The Journal of Chemical Physics*, 51(1), 133-136.

[46] Shliomis, M. I., & Morozov, K. I. (1994). Negative viscosity of ferrofluid under alternating magnetic field. *Physics of Fluids* (1994-present), 6(8), 2855-2861.

[47] Bacri, J. C., Perzynski, R., Shliomis, M. I., & Burde, G. I. (1995). "Negative-viscosity" effect in a magnetic fluid. *Physical review letters*, 75(11), 2128.

[48] Rosenthal, A. D., Rinaldi, C., Franklin, T., & Zahn, M. (2004). Torque measurements in spin-up flow of ferrofluids. *Journal of fluids engineering*, 126(2), 198-205.

[49] Sánchez, J. H., & Rinaldi, C. (2010). Magnetoviscosity of dilute magnetic fluids in oscillating and rotating magnetic fields. *Physics of Fluids* (1994-present),22(4), 043304.

[50] Suresh, A. K., & Bhalerao, S. (2002). Rate intensification of mass transfer process using ferrofluids. *Indian Journal of Pure and Applied Physics*, 40(3), 172-184.

[51] Olle, B., Bucak, S., Holmes, T. C., Bromberg, L., Hatton, T. A., & Wang, D. I. (2006). Enhancement of oxygen mass transfer using functionalized magnetic nanoparticles. *Industrial & engineering chemistry research*, 45(12), 4355-4363.

[52] Hajiani, P., & Larachi, F. (2013). Remotely excited magnetic nanoparticles and gas–liquid mass transfer in Taylor flow regime. *Chemical Engineering Science*, 93, 257-265.

[53] Hajiani, P., & Larachi, F. (2012). Reducing Taylor dispersion in capillary laminar flows using magnetically excited nanoparticles: Nanomixing mechanism for micro/nanoscale applications. *Chemical Engineering Journal*, 203, 492-498.

[54] Hajiani, P., & Larachi, F. (2013). Controlling lateral nanomixing and velocity profile of dilute ferrofluid capillary flows in uniform stationary, oscillating and rotating magnetic fields. *Chemical Engineering Journal*, 223, 454-466.

[55] Hajiani, P., & Larachi, F. (2014). Magnetic-field assisted mixing of liquids using magnetic nanoparticles. *Chemical Engineering and Processing: Process Intensification*.

[56] Rolland, M., Larachi, F., & Hajiani, P. (2014). Axial dispersion in nanofluid Poiseuille flows stirred by magnetic nanoagitators. *Industrial & Engineering Chemistry Research*.

CHAPTER II.

Inception of vortical coherent structures from spinning magnetic nanoparticles in rotating magnetic fields
New nanofluid microscale mixing tool[1]

O. **Gravel**[†], J. **Lauzon-Gauthier**[†], C. **Duchesne**[†], F. **Larachi**[†]

[†]Department of Chemical Engineering, Laval University, Québec, QC, Canada, G1V 0A6

[1] Gravel, O., Lauzon-Gauthier, J., Duchesne, C. & Larachi, F. (2014) Inception of vortical coherent structures from spinning magnetic nanoparticles in rotating magnetic fields ─ New nanofluid microscale mixing tool. *Chemical Engineering Journal* (submitted)

II.1. Résumé:

Afin d'approfondir la compréhension du phénomène de mélange résultant de l'interaction entre les champs magnétiques uniformes et les nanofluides magnétiques, une investigation optique des structures cohérentes générées par les nanoparticules magnétiques en rotation à l'intérieur de suspensions nanofluidiques diluées soumises à des champs magnétiques rotatifs est présentée. À cette fin, une technique de visualisation microscopique a été implémentée au centre d'un électro-aimant dans le but de permettre la capture d'images et de vidéos explicitant le comportement des nanofluides en champs magnétiques variables avec différents paramètres opératoires. Les effets d'une variation dans la fraction volumique en contenu magnétique, dans le diamètre des nanoparticules magnétiques, dans l'intensité et la fréquence des champs magnétiques rotatifs ainsi que dans le type de champ magnétique sur la génération de structures cohérentes ont été explorés. Les résultats découlant des observations ont ensuite été corrélés et analysés à l'aide d'un protocole multi-résolution de détection automatique des structures à différentes échelles basé sur les transformées bidimensionnelles orthogonales en ondelettes discrètes. Tous les paramètres pris en considération ont démontré un potentiel significatif d'altération des structures détectables au sein des nanofluides et ce avec différentes manifestations. En effet, chaque paramètre étudié correspond à des tendances et des seuils émergeant à différentes échelles pour différents types d'organisation. L'information ainsi obtenue ouvre maintenant la porte au réglage adéquat des paramètres d'une technologie de mélange microscopique fondée sur la rotation de nanoparticules magnétiques.

II.2. Abstract:

To improve understanding of the mixing phenomena resulting from the interaction between uniform magnetic fields and magnetic nanofluids, this work presents an optical investigation of the coherent structures generated by rotating magnetic nanoparticles in dilute nanofluid suspension submitted to uniform rotating magnetic fields. A microscopic visualisation technique was implemented inside the bore of an electromagnet to allow image and video capture of the variation in nanofluid behavior under time-varying magnetic fields and different operating parameters. The effects of magnetic core volume fraction, magnetic nanoparticle diameter, rotating magnetic field intensity and frequency as well as magnetic field type on coherent structure generation were explored. The observational results were subsequently correlated and analysed making use of an automatic structure detection protocol at different scales based on multi-resolution orthogonal 2-Dimensional discrete wavelet transforms. All the parameters considered were found to substantially affect detectable structure inception in the nanofluid in different ways, with trends and thresholds emerging for different types of organisation at different scales. This information now opens the door for adequate tuning of rotating magnetic nanoparticle based mixing technologies at the micro-scale.

II.3. Introduction:

In recent years, stable colloidal suspensions of magnetic nanoparticles (MNPs) have elicited a great deal of research, primarily in reason of the size and magnetic properties of the dispersed MNPs allowing for their manipulation at a distance by means of appropriate external magnetic fields [1-5]. Owing to this disposition, they have been involved in many applications where mixing at the micro-scale is a critical issue, e.g., catalytic reactions, separation, drug delivery and microfluidic devices [6-9]. In parallel, MNPs have also been studied for use as nanoscale devices to stimulate mixing in micro-scale when the whole system is subject to time-varying external magnetic fields [10-14]. The potential for mixing applications appears particularly remarkable for rotating magnetic fields (RMFs) although different magnetic fields have been considered [9-14].

Succinctly, this potential comes from the fact that external magnetic fields force the nanoparticles to align with field direction by exerting magnetic torque on the magnetic moment of MNPs suspended in liquids (or so called nanofluids) [15]. This torque is felt bodily for MNPs with a magnetic moment locked in the solid crystal structure, i.e., rigid-dipole rdMNPs, and the related momentum is transferable to the adjacent liquid phase [15]. Consequently, a time-varying magnetic field such as RMF with its ever changing directionality can exert an angular torque on MNPs, forcing gyration of the latter with respect to the surrounding liquid phase. In turn, provided the spinning MNPs are in a sufficiently dilute nanofluid suspension, where magnetic mutual interactions among MNPs are negligible [16-17], MNPs can transfer their momentum to the neighbouring liquid molecules and thus locally generate an angular motion (or nanoconvective streams) in the liquid.

However, while several studies used or investigated the effects of uniform magnetic fields on the physical behavior of MNP-laden fluids, interpretation of the resulting phenomenon usually has been made based on simulations or measurements performed indirectly or at a large scale [9, 14-18]. In order to fine tune the development of a mixing technology based on spinning MNPs in rotating magnetic fields, a clearer picture of the ferrohydrodynamics at play is required. For this purpose, the present work uses a microscopic visualisation

technique implemented inside of an electromagnet's bore in order to capture images of colloidal MNP-containing nanofluid suspensions sandwiched in thin micro-slides submitted to diverse magnetic fields. The visual repercussions of a change in suspension magnetic volume fraction, MNP diameter, RMF intensity and frequency as well as the use of equivalent oscillating and static magnetic fields (OMF & SMF) are investigated to shed light on the provenance of mixing quality and intensity. To support the derived interpretation, an image analysis protocol has been developed based on multi-resolution orthogonal wavelet analysis as a means to quantifiably assess the visual results.

II.4. Material and methods:

II.4.1. Magnetic field generation:

A tubular two-pole three phase electromagnet (1) (figure II.1a), with bore dimensions of 55 mm in height and 45 mm in diameter, was designed and fabricated in collaboration with MotionTech LLC (Arizona, USA) and Wingings Inc (Minnesota, USA). Its assembly consists of a magnet stator with three identical coil pairs, spatially shifted from each other by 120° in azimuthal direction. It is equipped with versatile power supplies for direct current (5), alternating current (3), rotating magnetic field generation (2), and a rectifier (4). This arrangement enables the generation of uniform RMFs, OMFs and SMFs of moderate magnetic field intensity at the central vertical axis (up to 50 mT) by energizing separately or jointly the three identical coil pairs composing the magnet in different configurations. The RMFs emerge from the superposition of three OMFs 120° out of phase, so for their generation the coils are energized by three balanced AC currents from a variable frequency drive (ABB, ACS150, 2.2 kW). The OMFs, for their part, are generated by two adjacent coils fed by alternating current from an AC variable frequency drive (Invertek Drives, Optidrive E2) while in the case of SMFs, the same adjacent coils are connected to direct current from a DC power supply (Agilent Tech, N8739A). The frequency and strength of the different magnetic fields are adjustable directly on the appropriate power supply. Temperature control of the magnet solid part is ensured by a jacket that encompasses the outer shell of the stator and is filled with equal volume parts of water and ethylene glycol circulating in and out from a constant-temperature thermostated bath (Lauda, Model

RKT20). More information on the specifications and design of the electromagnet can be found elsewhere [10].

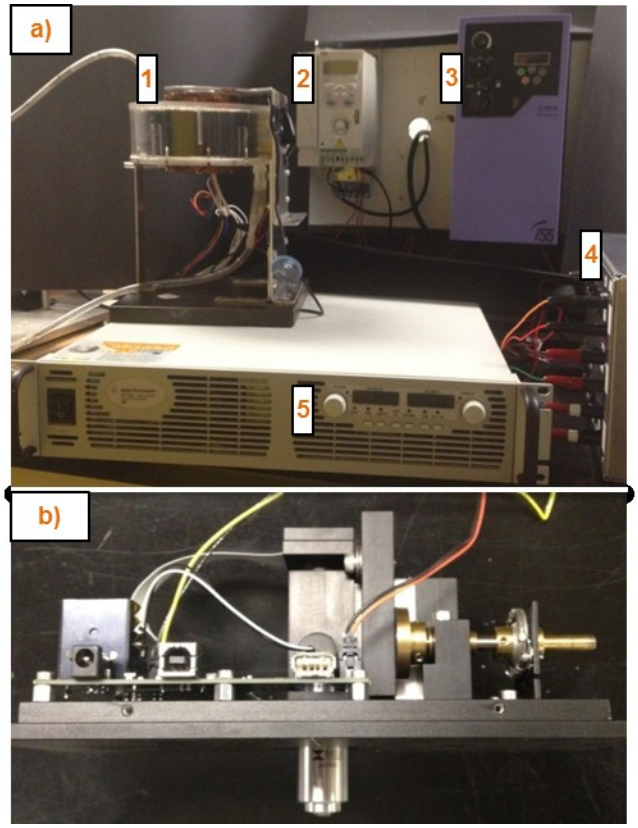

Figure II.1: a) Electromagnet setup and components: (1) Magnet , (2) RMF generation power supply, (3) AC power supply, (4) Rectifier, (5) DC power supply; b) Modified model 500 LumaScope^{TM} for insertion into magnet bore

II.4.2. Image capture:

Microscopic image acquisition was carried by the LumaView software from a modified model 500 LumaScope^{TM} from Etaluma Inc. (California, USA) which was disassembled and had its 40X objective inverted to allow for its insertion inside the electromagnet bore (figure II.1b). Microslides (100 µm x 1mm ID, 100 µm wall, 50 mm long slits) were filled with the fluid samples and laid flat at the center of the magnet, under the objective, with the plane of focus at 150 µm with respect to the slit upper face. Using standard bright field settings of sample illumination *via* transmitted white light across the slit thickness, grey-level images with a field of view of 640 µm × 400 µm and a pixel size of 0.5 µm were

collected at 0.2 sec intervals. The images can then be strung back together to create short videos displaying the discernable dynamic motion inside the fluid.

Such video files were prepared and are supplied as multimedia files in the electronic supplementary information section of this work. Accompanying the figures presented in the text, one video file was assembled for every parameter under scrutiny (magnetic core volume fraction, RMF intensity, RMF frequency, MNP diameter and magnetic field type) and contains a succession of one 10 second clip for each tested parameter value. These 10 second clips are composed of 50 captured images strung together at their acquisition rate (5 Hz) to accurately represent the observed phenomena. The image frame size was modified from 1280 x 800 pixels to 640 x 480 pixels to reduce file size while maintaining as much detail as possible in the videos.

II.4.3. Magnetic dispersions:

Diluted colloidal MNP suspensions with magnetic core volume fractions ranging from 0.001 v/v to 0.01 v/v were prepared from the commercially available water-based ferrofluids EMG705 from Ferrotec Inc., FluidMag-ARA from Chemicell Inc., and iron (II,III) oxide MNP solution from Sigma-Aldrich (725311-5mL) dispersed in deionized water. The magnetic properties of the ferrofluids were measured by an alternating gradient magnetometer, MicroMag model 2900 (Princeton Instrument Co.), at 298 K in low-field (for initial susceptibility, $\chi 0$) and high-field (for saturation magnetization, Ms) asymptotes of magnetization curve. From the obtained values, particle core diameters were estimated following a method proposed by Chantrell et al. [19]. While the three types of nanoparticles are characterized by superparamagetic magnetization, as opposed to the uncoated single domain magnetite MNPs stabilized by surfactants in EMG705 and Sigma-Aldrich solution, the larger particles in FuidMag-ARA are composed of a multi-domain magnetite core coated with a layer of glucuronic acid. This layer has to be added to the previously calculated core size to meet the advertised particle size of 200 nm. In the present case, this verification was subsequently made by measuring the hydrodynamic diameter of the undiluted ferrofluids' MNPs with a Zetasizer (model Nano 6, Malvern Intrsuments Ltd). This hydrodynamic diameter was found very close to 200 nm for FluidMag-ARA as stated by Chemicell, and slightly larger than the core MNP diameter for the two other fluids, once

again consistent with literature findings for such measurements. Table II.1 summarizes the properties of the original as-received undiluted ferrofluids. Finally, although it was determined that cluster or chain formation during the course of experiments was highly unlikely at the utilized dilute concentrations [16, 17], to verify particle stability throughout testing, particle size distributions for the employed concentrations of the different MNPs were also measured with the Zetasizer from samples before and after exposure to magnetic fields. No statistically significant difference was found between the aforementioned samples, confirming the absence of clusters or chain formation during the experiments.

Table II.1: Magnetic properties of as-received (undiluted) ferrofluids

Ferrofluid	EMG 705	FluidMag-ARA	Sigma-Aldrich
Saturation magnetization, M_s	18.7 kA/m	1.43 kA/m	64.5 A/m
Initial susceptibility, χ_0	2.9	0.074	0.0038
MNP volume fraction, ϕ	0.042 v/v	0.01125 v/v	0.0012 v/v
Median magnetic core diameter, d_p	16 nm	181 nm	5 nm
Hydrodynamic diameter, d_h	24.8 ±7.25 nm	204.9 ±12.15 nm	6.6 ±1.41 nm

II.4.4. Image analysis:

Quantitatively, the discernible coherent structures in the collected images were evaluated using a protocol based on multiresolution orthogonal wavelet analysis. Wavelet transforms are a useful tool in image analysis to study complex phenomena at different scales [20] by reason of the possibility to investigate the spatial and frequency relationship occurring in an image due to its decomposition into different frequency components and their analysis using a resolution adapted to the scale [21]. For example, high frequency variations (i.e. high pixel intensity contrast) from pixel-to-pixel yields a fine texture whereas lower frequency variations (i.e. intensity contrast between pixels at larger distance from each other) leads to coarser textures. Consequently, they are well suited for detection in a fluid with dynamics displaying complex structures counting a wide range of coexisting scales and a variety of shapes [22, 23].

More precisely, in the present case the 2-Dimensional Discrete Wavelet Transform (2D-DWT), a state-of-the-art multi-resolution image texture analysis method developed in the

image processing field, was used [24]. Since the wavelets have a finite length, as opposed to the infinite length sine and cosine functions of the Fourier Transform, this method is able to perform a spatial-frequency decomposition of the image through a convolution between the image signals and the wavelet function.

The first step of this approach consists of selecting the type and length of the wavelet, also called mother wavelet. There are several wavelet families described in the literature and, in general, the choice is not unique as many wavelets can perform equally well on a given set of images [20]. The spatial-frequency decomposition is obtained by dilating the mother wavelet and translating it across the images. Doing so, it captures information at different frequencies that are decreasing as the scale of the wavelet increases.

The 2D-DWT performs the scaling of the wavelet not by dilating the mother wavelet itself, but by downsampling the rows and columns of the image by a factor of two at each decomposition level (i.e., dyadic downsampling). The wavelet is convoluted with the image at each scale of decomposition and the fit between the wavelet and the image signal is computed for every pixel. This is done in the horizontal, vertical and diagonal directions. The length of the wavelet allows capture of the spatial information and the scaling of the images captures the frequency information. The computed correlations between the wavelet and the image are called detail coefficients. The output of 2D-DWT at scale *s* is a set of three detail sub-images D_{sH}, D_{sV}, $D_{sD,}$ representing the information captured by the wavelet in all three directions, and the approximation sub-image A_s, representing the information discarded by the wavelet. The procedure is then repeated for a selected number of scales (s=1,2,…S). The detail sub-images can be viewed as results of a band pass filtering and the approximation is the result of a low pass filter. The scale of decomposition is inversely proportional to the frequency. The detail sub-images at the first scale will capture high frequency information, or small size structures, and higher scales will contain lower frequency information and thus bigger structures. Interested readers can refer to Mallat [21] for more details on the method.

In this study, the Daubechies mother wavelet was chosen for being a family of orthogonal functions that are easily adapted to soft images in terms of low frequencies [20] and for their stability and ease of inversion, providing an easy and efficient reconstruction of the

image [24]. The orthonormal wavelet families from which they are a part have also been shown to adequately decompose turbulent flow images when using more than 10 coefficients [23], meaning with index numbers higher than 10, so after trials the Daubechies wavelet of index 18 was selected for the task at hand. Furthermore, the chosen decomposition was made in 6 levels to allow for a clear differentiation between them, and only the five with lower energy (levels 2 to 6), thus containing the coarser textures were kept in the subsequent steps of analysis since the details in the first level were too small to take into account.

For every experimental test, the processing was started by selecting 151 consecutive images in which the fluid behaviour is deemed in a steady-state condition. For every image, the first step of analysis is normalization of the grey level values, placing all the tests on equal footing, followed by decomposition into wavelet components in order to obtain the wavelet approximation coefficients (i.e., results of the low pass filtering $\mathbf{A}_i$) for each of the six levels. The next step is application of the inverse wavelet transform to reconstruct the images at each scale using only the approximation coefficients. This results in a series of images each capturing different sizes of visible structure from smaller size to bigger size as the decomposition level increases. The resulting grey level images are subsequently thresholded using Otsu's method [26] and converted to intensity images (T_i) to allow for automatic object detection. To avoid detecting the same structures in different image scales, the difference between two scales was used for quantifying the size distribution of the structures. The higher levels were subtracted from the lower ones, keeping only the new features with each descending scale of higher energy. That is, the thresholded approximation image T_{i-1} was subtracted from image T_i to keep only the structures not detected in T_i. This gives a series of 5 structure images (S_i where i = 2: 6). An example of thresholding and subtraction steps for the 5^{th} and 6^{th} decomposition levels of an image can be seen in figure II.2. An automatic element detection algorithm was then used to quantify the results by counting and measuring the area of the structures detected at every level for each image of a test. The subsequent step is then noise removal from the collected data by discarding the structures detected with a size under 2X2 pixels corresponding to an area of 1 μm^2 based on Nyquist–Shannon sampling theorem since the minimum resolution of the camera is 0.5 □m. Finally, the mean element area of the resulting structure area distribution

as well as the total number of detected elements for the 151 images in each tests are computed to graphically compare the different scenarios.

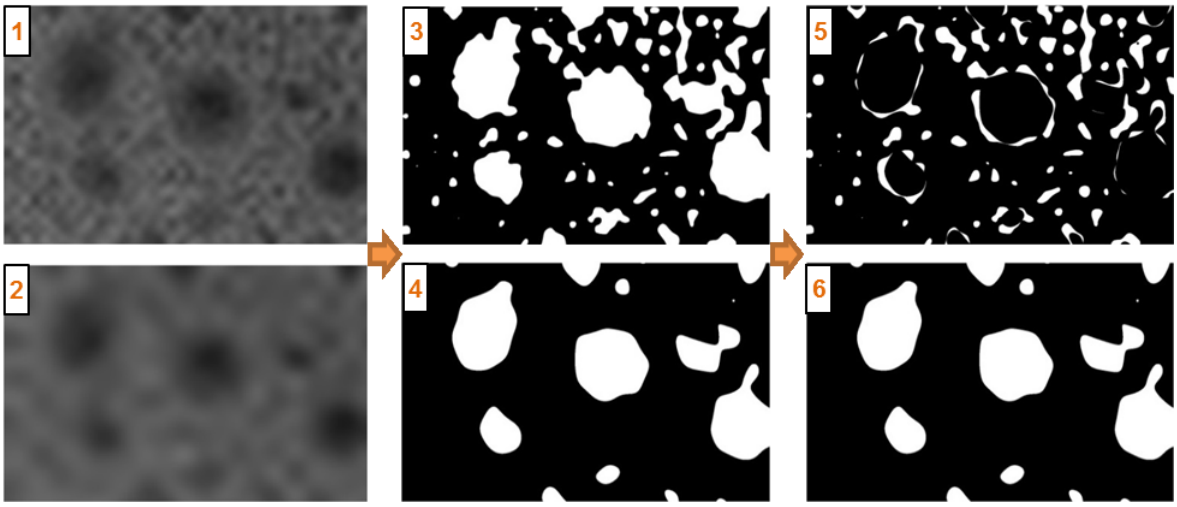

Figure II.2: Sample of the thresholding and subtraction steps for the 5th and 6th decomposition levels of an image : (1) Reconstructed image from 5th level approximation coefficients, (2) Reconstructed image from 6th level approximation coefficients, (3) (4) Thresholded images for the respective levels, (5) Image resulting from the subtraction of (4) to (3), sent to the automatic element detection algorithm for the 5th decomposition level, (6) Unchanged 6th decomposition level thresholded image sent for detection since there is no higher level

II.5. Results and discussion:

In order to adequately investigate the effect of the parameters at play in the rotation of MNPs in suspension, every parameter was investigated independently on a range adequate for the available fluids and the setup. Magnetic core volume fraction was scrutinized from 0.001 to 0.01, RMF intensity from 10.4 kA/m to 31.4 kA/m, RMF frequency from 10 Hz to 200 Hz, MNP size from 5 nm diameter to 200 nm and corresponding rotating, oscillating and static magnetic fields were also evaluated.

Since the average distance between MNPs is several times greater than their diameter at the employed magnetic core volume fractions (from 129 nm to 60 nm for d_p = 16 nm) [15], mutual interactions between MNPs may be neglected [16, 17] and the resulting phenomena can be interpreted as arising from the action of isolated nanoparticles under magnetic field. In the absence of magnetic field, the net (ensemble-average) spin vector is equal to zero because of the randomized MNP magnetic moments in all directions due to Brownian

agitation. Conversely, as soon as MNP magnetic torque overcomes thermal agitation (as well as mechanical viscous torque) as a result of a sufficient RMF strength, the particles undergo rotational reorientation, forcing them to spin perpendicular to the applied magnetic field. The rotating MNPs transmit kinetic energy to the embracing liquid and initiate nanoconvective flows therein as a result [13].

Examination of the collected images enables to shed light on some of the intrinsic differences in the fluid behavior resulting from the RMF induced rotation of MNPs in the different studied conditions. Starting with varying magnetic volume fraction displayed in figure II.3 (and in available video file ‘‘31042-vidII-1’’, submitted separately), the lowest value, 0.1% v/v (a, Clip 1), predominantly sees the emergence of well defined, relatively small (average $d \approx 7.6$ μm) vortical structures in front of a seemingly static background. At MNP concentration of 0.25% v/v (b, Clip 2), already the background looks more chaotic, and among the small structures analogous to the ones seen at the previous concentration, vortices of a second larger scale, with softly fading edges, are discernable. A turning point appears to be reached at 0.5% v/v (c, Clip 3), with the absence of a clear background as the whole field of view is populated by coherent structures in the form of darker shades of grey showcasing superior agitation state presumably because of greater instantaneous mean MNP concentration. Furthermore, larger scale vortices are now increasingly defined and noticeable in a larger number. The change is then clear from this concentration to the 1% v/v magnetic core volume fraction (d, Clip 4) where the complete field of view is vigorously in motion owing to vortical flows reminiscent of the dark grey shade and dynamics of the previous concentration’s large vortices inner area. These observations are supported by the multi-resolution wavelet analysis of the acquired images (e) showing a nearly exponential growth of the mean area of the detected structures with increasing MNP volume fraction along with linearly decreasing number of structures detected. Altogether, the results support the interpretation that increasing MNP concentration shrinks the length scale of the domain separating the agitated spheroid encompassing the particles. This entices short-range vortical structures to collide and organize, for an equivalent amount of dissipated energy from the particles, into larger structures culminating in a more intense mixing phenomenon. An analogy can be drawn with eddy coalescence in classical fluid dynamics [27], where coalescence of rotating liquid

spheroid regions occurs at some overlapping point. Based on their size (5 nm to 200 nm), the individual MNPs being obviously below the visible light range only the resulting larger scale structures, no smaller than 1 μm^2, can be discernable.

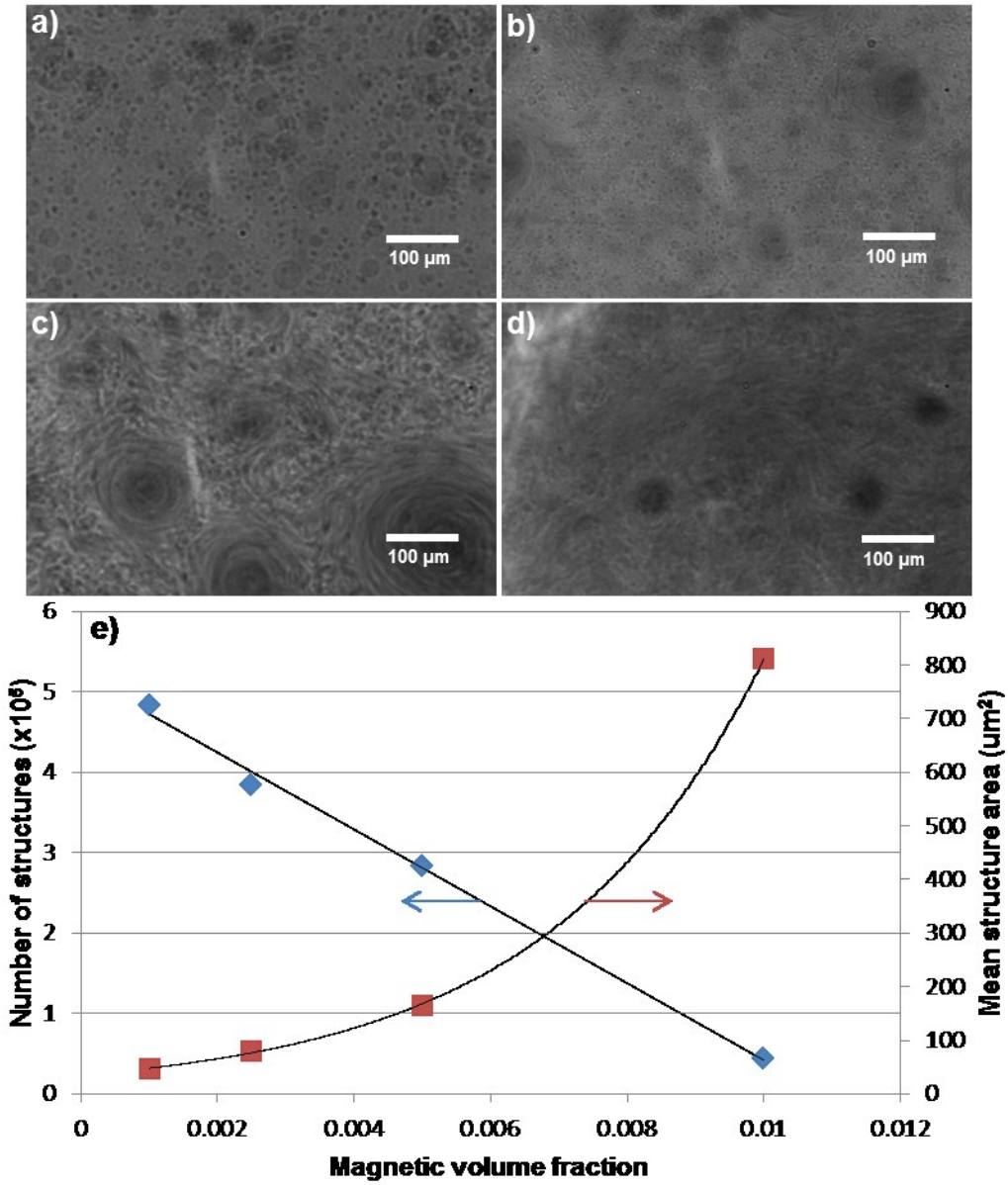

Figure II.3: 16 nm diameter MNPs submitted to a uniform RMF at 31.4 kA/m and 100 Hz for magnetic volume fractions of a) 0.001 b) 0.0025 c) 0.005 d) 0.01. e) Trends for the total number of detected structures and the associated mean area for the different magnetic volume fractions from the 2D-DWT analysis. The error bars are here too small to extend from the points

The differences are more subtle when it comes to a variation in RMF intensity presented in figure II.4 and in the video file ‘‘31042-vidII-2’’. The apparent changes here lie in the contrast at the boundaries of the small structures populating the background as well as the distinctness of the larger vortices. Compared to higher intensities, the emerging apparent vortical structures at 10.4 kA/m (a, Clip 1) are smaller in size and of a brighter shade, indicating a lower local amount of MNPs in the structures or a weaker motion of the ones composing them. The same underlying cause is also manifest in the larger vortices that, while similar in size to the ones in the subsequent intensities, are characterized by a clear gradual decline of their shade from center to boundaries. From this point to 31.4 kA/m ensues a progression towards slightly larger and more sharply delimited structures with the more imposing ones being increasingly homogeneously shaded (b, Clip 2 and c, Clip 3). Such a display is understandable since axial spinning of MNPs is magnetic-torque driven [15], and once again the observations are supported by the results of the wavelet analysis (d), with the mean surface of the detected structures almost linearly doubling between the lowest and highest intensity while the total number of structures shows a 24.3% linear decrease.

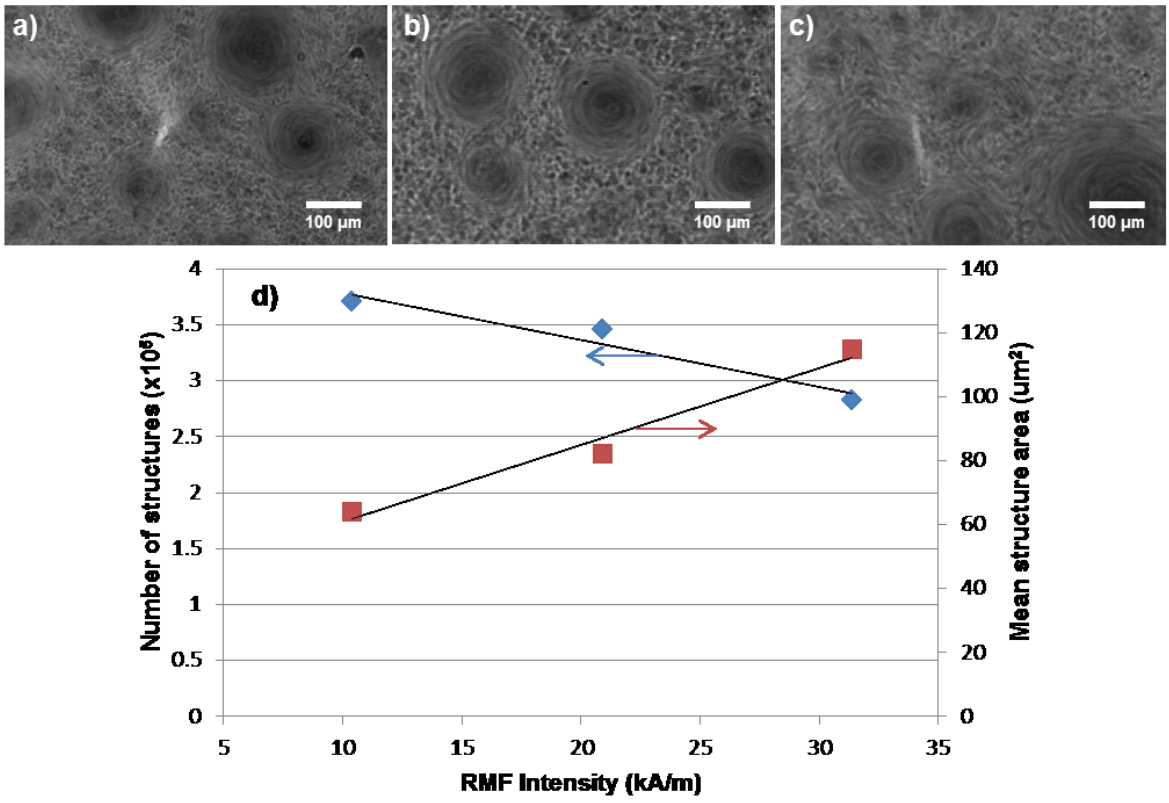

Figure II.4: 0.005 magnetic volume fraction suspension of 16 nm diameter MNPs submitted to a uniform RMF of 100 Hz with an intensity of a) 10.4 kA/m b) 20.9 kA/m c) 31.4 kA/m. d) Trends for the total number of detected structures and the associated mean area for the different RMF intensities from the 2D-DWT analysis

In the case of frequency variations presented in figure II.5 as well as in the video file ‘‘31042-vidII-3’’, the visual result is here clearly discernible. Indeed, at 10 Hz (a, Clip 1), although there is a definite agitating motion arising from the rotating MNPs noticeable in the small scale structures, the amount of torque transferred from the MNPs at this frequency does not seem to be substantial enough to initiate generation of superior-order coherent vortical structures. Curved, blurry contours following the arrangement of minute structures in a circular-like flow pattern are appearing instead. At 50 Hz (b, Clip 2), the background structures increased to a more appreciable size and no flow line is detectable. However, the entire field of view is occupied by vortical structures of the same order, indicating that the rotation speed and the related transferred torque is still insufficient to generate distinctly delimited larger-scale vortices although the vague, blurred outlines of such structures in formation can be sighted in several images and is evident in Clip 2 of the

video file. The threshold for the emergence of these larger, well-defined structures has decidedly been surpassed at 100 Hz (c ,Clip 3) while the background structures also significantly gained in sharpness and size. Once at 200 Hz (d, Clip 4), the difference is this time less salient in the vortical structures proportion than in their smoothness or homogeneity. The increased MNP rotation speed translates into visual elements moving perceptibly faster, foreground vortices having clearly defined borders and a backdrop seemingly vigorously agitated. These visual interpretations are seconded by the quantitative results (e) revealing the mean surface of the detected structures to follow an ascending linear trend until 100 Hz, where it heads towards a plateau. The number of detected structures for its part slowly decreases of 4% between 10 Hz and 100 Hz then drops to 43% of its original value at 200 Hz. These trends are explainable by the notable homogeneity brought by fast vortex coalescence and coarsened particle-encompassing solvent spheroids plausibly stemming from the increased MNP rotation speed at the highest frequency.

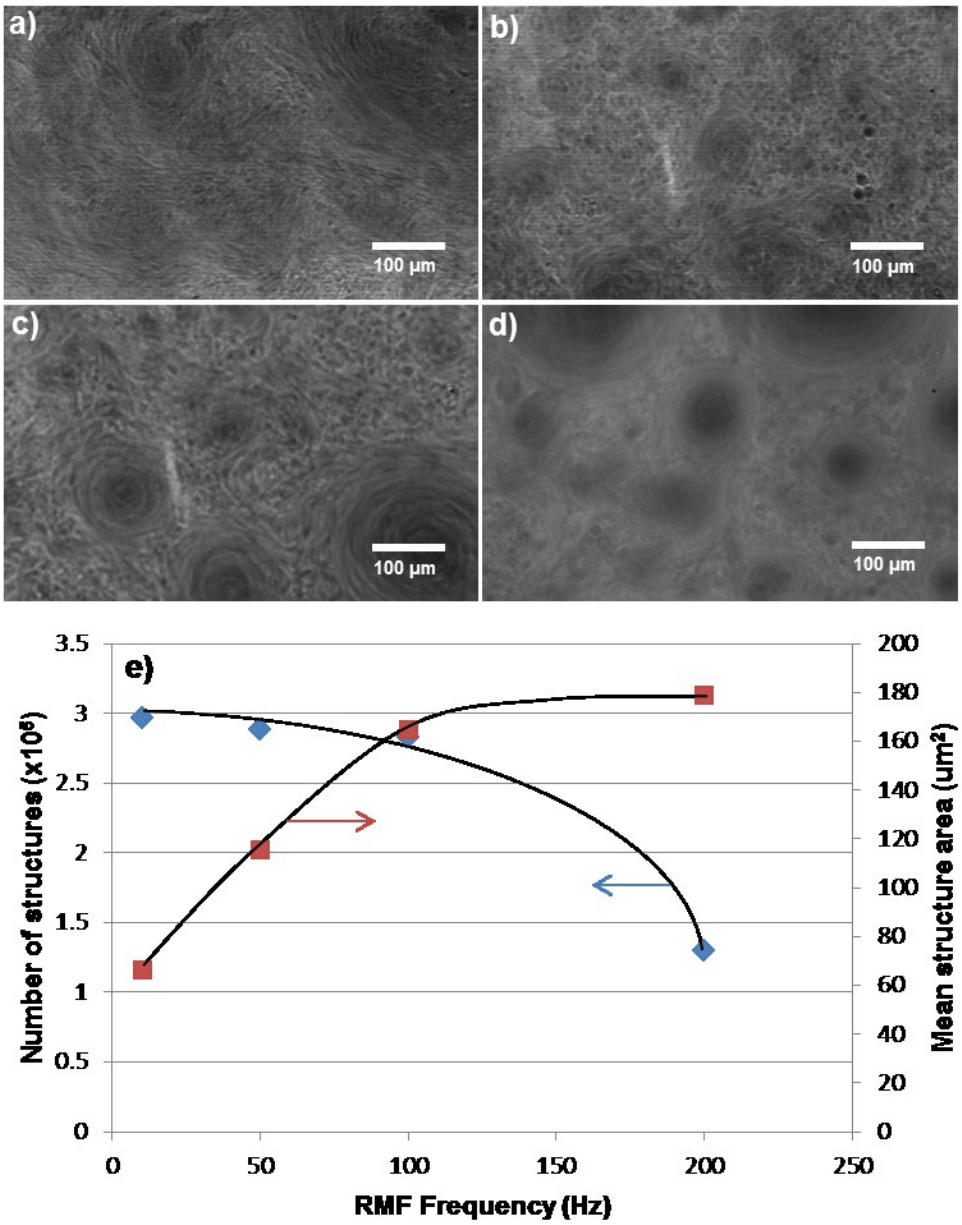

Figure II.5: 0.005 magnetic volume fraction suspension of 16 nm diameter MNPs submitted to a uniform RMF of 31.4 kA/m with an frequency of a) 10 Hz b) 50 Hz c) 100 Hz d) 200 Hz. e) Trends for the total number of detected structures and the associated mean area for the different RMF frequencies from the 2D-DWT analysis

The variation in size of the MNPs employed for an equivalent magnetic core volume fraction in the suspensions (figure II.6 and ‘‘31042-vidII-4’’) had to be investigated at the lower end of the concentration spectrum as the Sigma-Aldrich supplied suspension had an initial concentration only slightly above 0.1% v/v. As a result of the low magnetic core

volume fraction as well as their small size, the 5 nm MNPs (a, Clip 1) could not generate significant discernable structures at the scale probed by the current microscope. Although there is a detectable motion in the fluid under magnetic field evident in the related clip of the video file and the rotating action is inferable from the perceptible motion of impurities in the suspension, a visual interpretation of the result at this size is inaccessible except for the safe assumption that the inter-particle distance for this MNP size and concentration combination is too large to lead to vortex overlap and coalescence up to a detectable scale. The picture is quite different for 16 nm particles (b, Clip 2), still in the mono-domain range, where explicit vortical structures are detectable with a seemingly uneven size distribution and a calm, homogeneous backdrop. This contrasts with the perceivable structures generated from the rotation of multi-domain 200 nm MNPs (c, Clip 3), present in greater numbers and almost entirely covering the field of view, more narrowly distributed in size and apparently smaller. These findings can be correlated with the results from the multi-resolution wavelet analysis (d) exhibiting a decrease in the mean surface of the detected structures with an increase in their number as the diameter of the particles goes up. Visually as well as quantitatively, the larger particles seem to provide a more intense agitation, but while the effect looks stronger and covers a larger total area for the 200 nm MNPs, the superior order structures themselves are not larger, as is the case with other parameters, denoting a possible variation in the way these MNPs absorb magnetic energy and deliver it to the surrounding liquid.

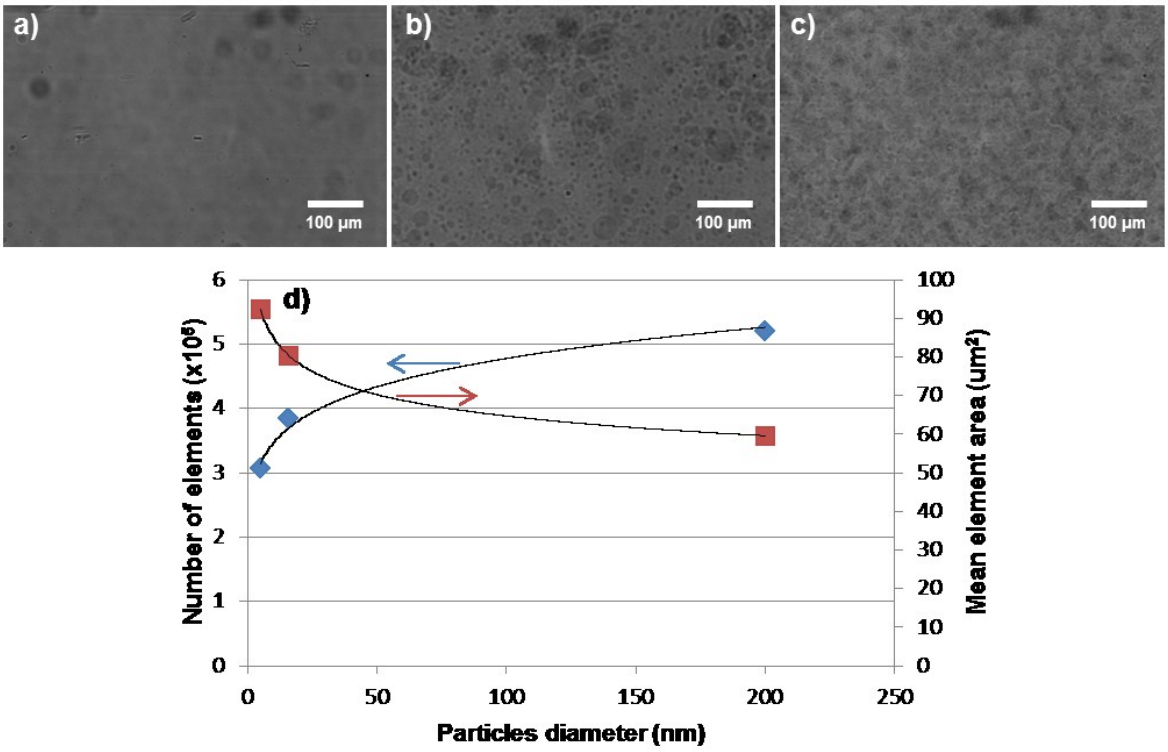

Figure II.6: 0.001 magnetic volume fraction MNP suspensions submitted to a uniform RMF of 31.4 kA/m and 100 Hz for different particle diameters of a) 5 nm b) 16 nm c) 200 nm. d) Trends for the total number of detected structures and the associated mean area for the different MNP diameters from the 2D-DWT analysis

The tests carried out under the two other magnetic field types are presented here in figure II.7 and in ‘‘31042-vidII-5’’ principally for visualization purposes, as the resulting structures and their organization under OMF (b, Clip 2) and SMF (c, Clip 3) diverge too much from the ones identified under RMF (a, Clip 1) to be acceptably quantifiably comparable. Nonetheless, a simple glance is enough to realize that the generated structures considerably differ from RMF to the two subsequent field types. The oscillating and static fields have been applied diagonally to with respect to the micro-slides and the field of view to avoid visual interferences from the images pixel lines or the screen scanning refresh rate during the course of experiment. The discernable structures under OMF and SMF are linearly organized and oriented in the magnetic field direction, and even though a vibration is perceptible under OMF, the whole looks fairly static in comparison with the results under RMF. This effect can be interpreted in the light that, as opposed the constant rotating magnetic field, when coil electrical current and resultant OMF pass through zero prior to

changing direction, a brief time lapse prevails with a magnetic field of almost zero. During this moment, relaxed MNPs are free to rotationally diffuse by random Brownian collisions with the solvent molecules. The time scale, upon magnetic field removal, during which MNPs get disoriented by 180° from magnetic field direction due to Brownian collisions is called Brownian relaxation time constant [28] and is of the order of 10^{-5} s in the present experiments [29] while at the same time the OMF half-period is of 0.005 s. Since the reshuffling of magnetic moments from Brownian agitation occurs much faster than the OMF half-period, it guarantees the randomness of nanoparticle spin directions during magnetic reorientation towards the opposite direction, thus resulting in zero average-spin velocity per unit volume. Such nanoparticle intermittent spin is isotropic and so cannot give rise to vortical structures as seen under RMF. Comparatively, the SMF locks MNPs in the magnetic field direction, creating similar but less intense linear structures due to the absence of continual back and forth motion.

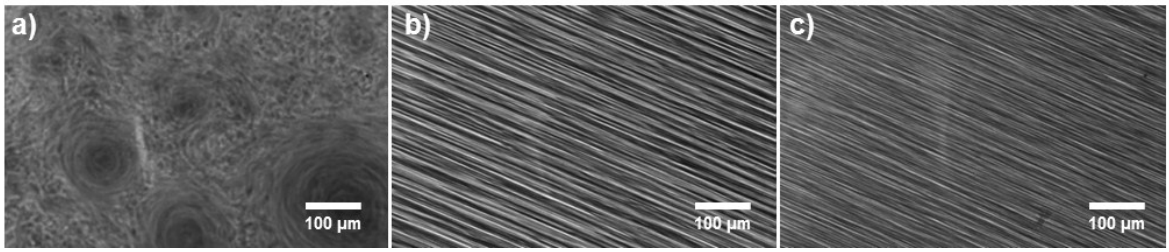

Figure II.7 : 0.005 magnetic volume fraction suspension of 16 nm diameter MNPs different types of uniform magnetic fields of 31.4 kA/m. a) RMF, 100 Hz b) OMF, 100 Hz c) SMF

II.6. Conclusion:

In order to gain more insight into the effects of magnetic fields on the behavior of water suspended magnetic nanoparticles for the development of a mixing technology in the context of microfluidic applications, the microscopic visualisation technique developed in this study was implemented at a small scale directly inside of the magnetic fields. It allowed probing the observable repercussions of oscillating, static, and especially rotating magnetic fields on the MNP motion-generated coherent structures in dilute suspensions with respect to the field parameters. Furthermore, an innovative use of a multi-resolution

orthogonal wavelet analysis coupled with a particle detection and measurement algorithm was made to quantify the captured results and provide a thorough assessment of the physical quality and behaviour of the coherent vortical structures emerging from the rotation of MNPs subjected to RMFs. The application of 2-Dimensional discrete wavelet transforms created the possibility to separate the structures apparent in different information frequency ranges in order to increase the efficiency of the automatic detection algorithm along with providing multiple comparative bases for the sets of images. This was in turn able to quantifiably support the observations elicited from the visual analysis and indicate the differences stemming from the parameters on the generation of larger scale structures. An increase in magnetic core volume fraction was found to greatly intensify the size and coverage of the emerging coherent vortical structures, and so is the case for increasing the frequency or the intensity of the applied RMF. The size of the MNPs in the suspension also affected the scale and distribution of the perceptible structures, as bigger particles were found to generate slightly smaller structures, but in a larger number and with a narrower size distribution. Finally, the sharp difference between RMF, OMF and SMF was illustrated, with the change from the circular vortical structures of RMF to linear, quasi-static structures for the two other field types, echoing the magnetization behaviour of the individual nanoparticles in these fields. Finally, the extracted information shows potential and provides a new path in the quest for the development and tuning of a versatile mixing technology for microfluidic devices based on the rotation of MNPs under RMFs. Future interesting work would try to predict and simulate MNP behavior to replicate the phenomena behind the emergence of the coherent vortical structures observed under RMF in order to correlate the results with the established paradigm of ferrohydrodynamics [15].

II.7. Acknowledgements:

Support from the Natural Sciences and Engineering Research Council of Canada and the Canada Research Chair “Green processes for cleaner and sustainable energy” is gratefully acknowledged.

II.8. References:

[1] Sun, C., Lee, J. S., & Zhang, M. (2008). Magnetic nanoparticles in MR imaging and drug delivery. *Advanced drug delivery reviews*, *60*(11), 1252-1265.

[2] Singamaneni, S., Bliznyuk, V. N., Binek, C., & Tsymbal, E. Y. (2011). Magnetic nanoparticles: recent advances in synthesis, self-assembly and applications. *Journal of Materials Chemistry*, *21*(42), 16819-16845.

[3] Lee, J. H., Jang, J. T., Choi, J. S., Moon, S. H., Noh, S. H., Kim, J. W., ... & Cheon, J. (2011). Exchange-coupled magnetic nanoparticles for efficient heat induction. *Nature Nanotechnology*, *6*(7), 418-422.

[4]Polshettiwar, V., Luque, R., Fihri, A., Zhu, H., Bouhrara, M., & Basset, J. M. (2011). Magnetically recoverable nanocatalysts. *Chemical reviews*, *111*(5), 3036-3075.

[5] Giouroudi, I., & Kosel, J. (2010). Recent progress in biomedical applications of magnetic nanoparticles. *Recent patents on nanotechnology*, *4*(2), 111-118.

[6] Pamme, N. (2012). 10 Magnetic Nanoparticles in Lab-on-a-Chip Devices.*Magnetic Nanoparticles: From Fabrication to Clinical Applications*, 277.

[7] Indira, T. K., & Lakshmi, P. K. (2010). Magnetic nanoparticles—A review. *Int. J. Pharm. Sci. Nanotechnol*, *3*(3), 1035-1042.

[8] Lee, S. H., van Noort, D., Lee, J. Y., Zhang, B. T., & Park, T. H. (2009). Effective mixing in a microfluidic chip using magnetic particles. *Lab on a Chip*,*9*(3), 479-482.

[9] Zhu, G. P., & Nguyen, N. T. (2012). Rapid magnetofluidic mixing in a uniform magnetic field. *Lab on a Chip*, *12*(22), 4772-4780.

[10] Hajiani, P., & Larachi, F. (2012). Reducing Taylor dispersion in capillary laminar flows using magnetically excited nanoparticles: Nanomixing mechanism for micro/nanoscale applications. *Chemical Engineering Journal*, *203*, 492-498.

[11] Hajiani, P., & Larachi, F. (2013). Controlling lateral nanomixing and velocity profile of dilute ferrofluid capillary flows in uniform stationary, oscillating and rotating magnetic fields. *Chemical Engineering Journal*, *223*, 454-466.

[12] Hajiani, P., & Larachi, F. (2013). Remotely excited magnetic nanoparticles and gas–liquid mass transfer in Taylor flow regime. *Chemical Engineering Science*, *93*, 257-265.

[13] Hajiani, P., & Larachi, F. (2013). Giant effective liquid-self diffusion in stagnant liquids by magnetic nanomixing. *Chemical Engineering and Processing: Process Intensification*, *71*, 77-82.

[14] Rolland, M., Larachi, F., & Hajiani, P. (2014). Axial dispersion in nanofluid Poiseuille flows stirred by magnetic nanoagitators. *Industrial & Engineering Chemistry Research*, 53, 6204-6210

[15] Rosensweig, R. E. (2013). *Ferrohydrodynamics*. Courier Dover Publications.

[16] Gubin, S. P., Koksharov, Y. A., Khomutov, G. B., & Yurkov, G. Y. (2005). Magnetic nanoparticles: preparation, structure and properties. *Russian Chemical Reviews*, *74*(6), 489.

[17] Yang, H. T., Liu, H. L., Song, N. N., Du, H. F., Zhang, X. Q., Cheng, Z. H., ... & Li, L. F. (2011). Determination of the critical interspacing for the noninteracting magnetic nanoparticle system. *Applied Physics Letters*, *98*(15), 153112-153112.

[18] Torres-Díaz, I., Rinaldi, C., Khushrushahi, S., & Zahn, M. (2012). Observations of ferrofluid flow under a uniform rotating magnetic field in a spherical cavity.*Journal of Applied Physics*, *111*(7), 07B313.

[19] Chantrell, R. W., Popplewell, J., & Charles, S. (1978). Measurements of particle size distribution parameters in ferrofluids. *Magnetics, IEEE Transactions on*,*14*(5), 975-977.

[20] Goswami, J. C., & Chan, A. K. (2011). *Fundamentals of wavelets: theory, algorithms, and applications* (Vol. 233). John Wiley & Sons.

[21] Mallat, S. G. (1989). A theory for multiresolution signal decomposition: the wavelet representation. *Pattern Analysis and Machine Intelligence, IEEE Transactions on*, *11*(7), 674-693.

[22] Farge, M. (1992). Wavelet transforms and their applications to turbulence.*Annual Review of Fluid Mechanics*, *24*(1), 395-458.

[23] Li, H. (2001). Visualization of a turbulent jet using wavelets. *Journal of Thermal Science*, *10*(3), 211-217.

[24] Nason, G. (2010). *Wavelet methods in statistics with R*. Springer.

[25] Meyer, Y. (1993). Wavelets-algorithms and applications. *Wavelets-Algorithms and applications Society for Industrial and Applied Mathematics Translation., 142 p.*, *1*.

[26] Otsu, N. (1975). A threshold selection method from gray-level histograms. *Automatica*, *11*(285-296), 23-27.

[27] Laufer, J. (1975). New trends in experimental turbulence research. *Annual Review of Fluid Mechanics*, *7*(1), 307-326.

[28] Morrish, A. H. (2001). The physical principles of magnetism. *The Physical Principles of Magnetism, by Allan H. Morrish, pp. 696. ISBN 0-7803-6029-X. Wiley-VCH, January 2001.*, *1*.

[29] Chaves, A., Zahn, M., & Rinaldi, C. (2008). Spin-up flow of ferrofluids: Asymptotic theory and experimental measurements. *Physics of Fluids (1994-present)*, *20*(5), 053102.

CHAPTER III.

Magnetically-induced agitation in liquid-liquid-magnetic nanoparticle emulsions

Potential for process intensification[*]

O. **Gravel**[†], P. **Hajiani**[†], F. **Larachi**[†]

[†]Department of Chemical Engineering, Laval University, Québec, QC, Canada, G1V 0A6

[*] Olivier, G., Pouya, H., & Faïçal, L. (2013). Magnetically induced agitation in liquid-liquid-magnetic nanoparticle emulsions: Potential for process intensification. *AIChE Journal*. 60: 1176–1181

III.1. Résumé:

Les technologies de mélange microscopique mettant en oeuvre des nanoparticules magnétiques offre un potentiel considérable d'intensification des procédés chimiques dans lesquels la diffusion, dans des régions submicroniques, est une étape limitante. Nous souhaitons éviter un contact direct entre les nanoparticules magnétiques et la phase continue à mélanger. Nous étudions le comportement d'émulsions de ferrofluides de type huile dans l'eau afin d'obtenir une intensité de mélange égale à celle obtenue avec des suspensions colloïdales diluées des mêmes nanoparticules. Pour établir une comparaison, des mesures du couple exercé sur l'arbre d'un viscosimètre par des émulsions de ferrofluide d'une part et des suspensions colloïdales d'autre part, soumises à des champs magnétiques uniformes statiques, alternatifs et rotatifs sont effectuées. Les résultats obtenus permettent d'affirmer que l'intensité du mélange des deux types de solution présente la même amplitude et, pour des contenus magnétiques identiques, varie proportionnellement à l'intensité du champ magnétique appliqué pour les trois types de champs utilisés. Nous en déduisons que le moment des nanoparticules magnétiques en rotation dans les émulsions est suffisant pour être transmis aux gouttelettes de la phase organique qui les contient et ainsi qu'à la phase continue. Plus particulièrement, l'intensité de l'action des nanoparticules soumises aux champs magnétiques rotatifs (CMR) est suffisante pour envisager le développement d'une technologie de mélange versatile et robuste utilisant des agitateurs nanoscopiques distincts de la phase continue à mélanger.

III.2. Abstract:

Microscopic mixing using magnetic nanoparticles (MNPs) unveils exciting ramifications for process intensification in chemical engineering. The present study explores the use of oil-in-water MNP emulsions to achieve mixing in a non-magnetic continuous phase tantamount to that occurring in equivalent dilute ferrofluid suspensions. To assess the technique, measurements of the torque exerted by ferrofluid emulsions and suspensions of equal magnetic content were performed in rotating, oscillating and static magnetic fields. Results show that momentum transfer is fairly alike in amplitude and proportionality for the two types of systems of equal magnetic content under the three types of magnetic fields. This implies that momentum of spinning nanoparticles in the emulsions is transferable to the oil droplets containing them which, in return is then transferred to surrounding non-magnetic liquid. The magnitude of the resulting mixing allows for the foresight of a versatile MNP mixing technology completely separated from the target phase being mixed.

III.3. Introduction:

Stable colloidal suspensions of magnetic nanoparticles (MNPs) continue to be broadly studied as these enable the modification of liquid properties, especially when submitted to external magnetic fields [1, 2]. Indeed, they exhibit unique behavior compared to the bulk form of ferro or ferrimagnetic materials. The size-dependent properties of MNPs, especially their superparamagnetism that stem from their single-domain nature and their high specific surface area are considered to form the basis for the design of novel magnetically-stimulated techniques with multiple applications in chemical engineering, chemistry, biotechnology and medicine [3-6].

The modification and control of fluid properties principally stem from the transfer of electromagnetic energy from the MNPs to the liquid, resulting in the occurrence of noteworthy alterations of liquid magnetoviscous properties. For example, in a ferrofluid shear flow, it is known that an external magnetic field forces MNPs to spin asynchronously with respect to the local vorticity of the fluid, resulting in an anisotropic modification of viscosity.[7] This behavior, known as rotational viscosity, was identified and studied by ferrofluid body torque measurements in a cylindrical Couette geometry [8-11].

Recently, this energy transfer from the MNPs to the liquid has been put in use by converting the suspended particles into nanostirrers allowing control of mixing in nanoscale when the whole system is subject to rotating, oscillating and static uniform magnetic fields (RMF, OMF, SMF) [12, 13]. In doing so, it has been shown that rotating MNPs under transverse rotating magnetic fields (RMF) generates nanoscopic liquid eddies inducing enhancement of liquid transport properties beyond the conventional paradigm of molecular diffusion [12, 13].

However, conventional ferrofluids imply direct contact between surfactant-stabilized MNPs and a continuous liquid phase, e.g., solvent. This represents a severe impediment to implement (bio)chemical transformations directly in ferrofluids. As a matter of fact, preserving the MNP colloidal stability despite occurrence of potentially unwanted chemical interactions between the stabilizing surfactants and desirable (bio)chemical transformations is far from being a trivial task. In order to avoid this possibility while still taking advantage

of the magnetic, nanoscale mixing effect of MNPs, to promote mixing we propose the use of ferrofluid emulsions consisting of small immiscible ferrofluid droplets emulsified in a *non-magnetic* continuous phase [14, 15]. Currently, experimental evidence is lacking concerning magnetic torque transfer from the MNPs trapped inside the immiscible droplets of an emulsion to its surrounding continuous non-magnetic phase under magnetic field stimulation. The possibility for such bottom-to-up momentum transfer, if objectified, is expected to open up a range of new process intensification applications where MNP-bearing liquid inclusions can serve to mix, without interference, non-magnetic liquids where chemical transformations are running.

Consequently, we proposed to investigate the effects of different RMF, OMF and SMF on the body torque exerted by MNPs inside oil-based ferrofluid emulsions and to compare them to water-based ferrofluids with the same magnetic content. Our analysis allowed quantifying the amplitude of the force exerted by excited MNP action inside ferrofluid emulsions under different magnetic fields. The torque measurement tests with dispersed MNPs in organic phase of oil-in-water emulsions subjected to RMFs demonstrate that the momentum of spinning MNP is transferable to the droplets, and then to the continuous phase of the emulsion with comparable intensity to that of the same MNPs content dispersed in aqueous conventional ferrofluids.

III.4. Methodology:

III.4.1. Magnet:

The tubular electromagnet utilized in the setup was designed and fabricated in collaboration with MotionTech LLC and Wingings Inc. It is a two-pole three phase magnet, with bore dimensions of 55 mm in height and 45 mm in diameter equipped with a Brookfield LVII+Pro viscometer (Figure III.1a). The magnet assembly consisted of a versatile power supply for direct current (6), alternating current (7), rotating magnetic field generation (8), and a rectifier (9) (Figure III.1b). This assembly is used to generate uniform RMFs, OMFs and SMFs of moderate magnetic field intensity at the central vertical axis (up to 50 mT). The three identical coil pairs constituting the magnet can be energized separately or jointly in different configurations in order to generate the required magnetic field type. Since RMF

emerges from the superposition of three OMFs that are 120° out of phase, the coils were energized by three balanced AC currents from a variable frequency drive (ABB, ACS150, 2.2 kW). In the case of OMFs, two adjacent coils are fed by an AC current from an AC variable frequency drive (Invertek Drives, Optidrive E2). The same adjacent coils are connected to DC current from a DC power supply (Agilent Tech, N8739A) to generate SMFs. Magnetic field frequency and strength is adjustable directly on the different power supplies. The temperature of the magnet solid part is controlled by a water-cooled jacket that encompasses the outer shell of the stator and is filled with a coolant circulating in and out from constant-temperature thermostated bath (Lauda, Model RKT20). More information on the specifications and design of the electromagnet are given elsewhere [12].

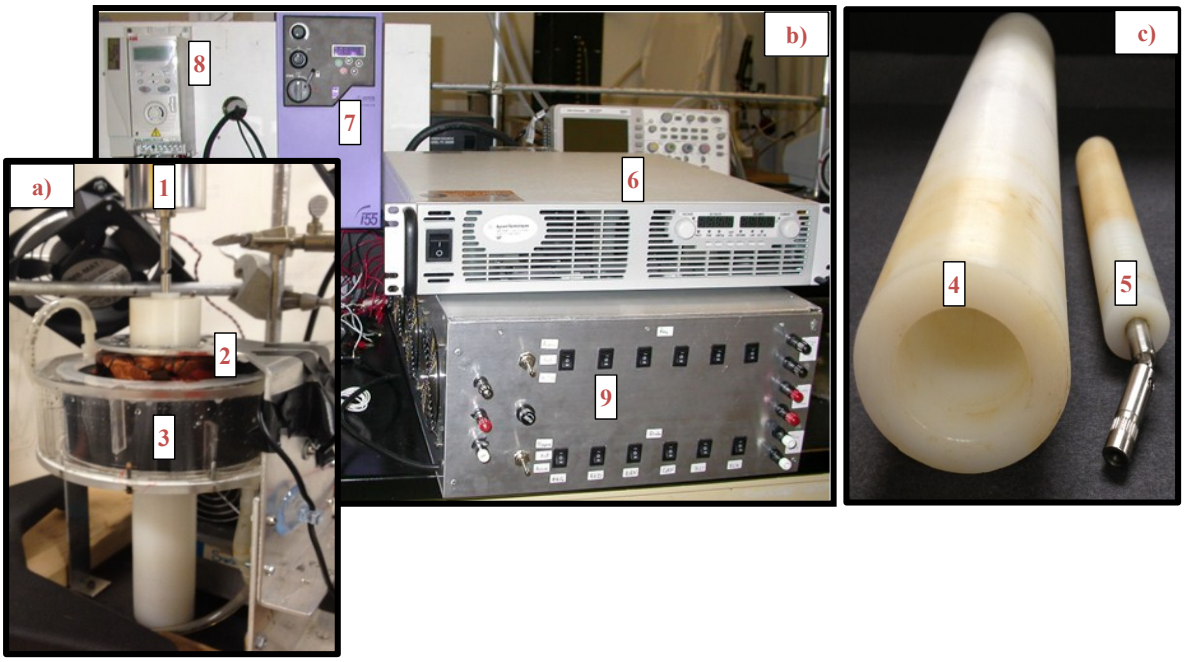

Figure III.1: Torque measurements experimental setup and components (a) Magnet device, (1) Brookfield LVII+Pro viscometer, (2) electromagnet, (3) cooling jacket; (b) magnet assembly and versatile power supply for (6) dc, (7) ac (8) rotating magnetic field generation, (9) rectifier; (c) ultra-high density polyethylene custom-made parts, (4) fluid container, (5) rotating spindle

III.4.2. Ferrofluid emulsions:

Oil-in-water type ferrofluid emulsions were prepared following a conventional procedure that has been proven to be an easy, cost effective and reliable way to obtain stable

emulsions [14, 16-19]. The ferrofluid used in the emulsions is an oil-based ferrofluid (EMG905 from Ferrotec Inc.) containing 8.1% by volume of Fe_3O_4 and the surfactant required to stabilize the oil-in-water emulsions is sodium dodecyl sulfate (SDS) of 99.9% purity from Bio-Rad. The first step of preparation consists of dissolving 5 g of SDS in 15 g of deionized water in order to produce a concentrated surfactant solution. A designated volume of this solution, necessary to obtain the final emulsion volume at 1.2 mmol/L of SDS, is then placed in a glass vial. In order to induce inversion during the emulsion preparation, this volume must be smaller than the volume of ferrofluid to be added, otherwise, only a fraction of the concentrated surfactant solution is initially placed in the vial and the rest is added later on. The next step consists of a very careful addition of the required amount of ferrofluid under constant mixing. Since the total volume at this point is relatively small, mixing is done using an ultrasonic bath (Ultrasonics Tru-Sweep model 275HTA) for 30 min. While maintaining mixing, the rest of the concentrated SDS solution or deionized water is then slowly and carefully added until inversion point, at which the completion to final emulsion volume with deionized water can be continued a little faster over the course of an hour. To finalize, the emulsion is transferred to a beaker and homogenized using an Omni Mixer Homogenizer for 3 h to reach maximum stability [17]. The droplet composition is obtained from EMG905 characterization (Table III.1) and the size of droplets in the resulting emulsions, given in Table III.2, is measured with a Zetasizer (Malvern, model Nano ZS). The initial mean diameter of the droplets was measured directly following preparation of the emulsions and the final mean diameter was measured once the tests were completed with a specific emulsion. In both cases, the samples were briefly agitated using a BR-2000 Vortexer from Bio-Rad prior to the measurements to ensure maximum homogeneity. The approximate number of MNP per droplet and the approximate mean distance between droplets were deduced from the initial size analysis data and the composition of the EMG 905 ferrofluid. Furthermore, the stability of the emulsions was assessed by the final mean diameter measurements shown in Table 2. An average size change of *ca*. 2.3% was determined after application of magnetic field and completion of the corresponding tests, indicating no significant change in droplet size.

Table III.1: Magnetic properties of as-received tested ferrofluids

Ferrofluid	EMG 905	EMG 705
Saturation magnetization, M_s	36.0 kA/m	18.7 kA/m
Initial susceptibility, χ_0	2.1	2.9
MNP volume fraction, ϕ	0.081 v/v	0.042 v/v
Median magnetic core diameter, d_p	12.4 nm	16 nm

Table III.2: Characterization of magnetic liquid-liquid-MNP emulsions

Magnetic content	Initial mean droplet diameter	Final mean droplet diameter	Approximate number of MNP/Droplet	Approximate mean distance between droplets
0.10 % v/v	158.2 nm	163.1 nm	311	1275 nm
0.25 % v/v	144.6 nm	148.4 nm	237	859 nm
0.50 % v/v	128.8 nm	130.2 nm	168	765 nm

To verify the distribution of magnetic nanoparticles inside the droplets, the prepared emulsions were observed under a JEOL JEM1230 transmission electron microscope (TEM) and the images were captured using a wide-field digital camera. The procedure consisted of a single drop of the emulsion deposited on a copper grid covered with a formvar–carbon membrane. A typical TEM micrograph of droplet MNP cargo from an emulsion of 0.10 % v/v magnetic content is illustrated in Figure III.2. Note that agglomeration shown was caused by the sample preparation and was reversible.

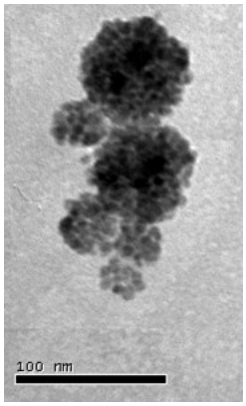

Figure III.2: TEM micrograph of droplets with their MNP cargo from the emulsion of 0.10 % v/v magnetic content. The reversible agglomeration shown was caused by the sample preparation

III.4.3. Colloidal MNP suspensions:

Diluted colloidal MNP suspensions with magnetic contents equivalent to those of the produced emulsions are prepared using the commercial water-based ferrofluid EMG705 from Ferrotec Inc. and deionized water. The magnetic properties of both ferrofluids (EMG705, EMG905) were measured by an alternating gradient magnetometer, MicroMag model 2900 (Princeton Instrument Co.), at 298 K in low-field (for initial susceptibility, χ_0) and high-field (for saturation magnetization, M_s) asymptotes of magnetization curve. Using these values, particle core diameter was estimated following a method proposed by Chantrell et al. [20].The results for the undiluted ferrofluids are presented in Table III.1 and originate from samples before and after exposure to magnetic fields, ensuring the absence of clusters or chain formation during the experiments.

III.4.4. Torque measurements:

Torque measurements are carried out using a Brookfield LVII+Pro (model LVDV-II+P) viscometer positioned at the center of the opening in the vertical axis of the magnet bore (3) (Figure III.1a). The viscometer is equipped with a custom built, ultra-high density polyethylene rotating spindle (5) with a diameter of 17.65 mm (Figure III.1c). A custom built container of the same material with an internal diameter of 27.45 mm (4) is placed inside the magnet containing 30 mL of ferrofluid. To initiate testing, the spindle is lowered into the liquid. The entire liquid (55 mm height) around the spindle is inside the magnet bore and exposed to the magnetic field.

In order to establish a comparison base, the first series of tests are performed in the absence of any magnetic field. The spindle rotation speeds ranged from 0.0036 s^{-1} to 3.5706 s^{-1}. After an initial stabilization time of 20 seconds for each set, 25 consecutive data points two seconds apart are collected. Data acquisition, performed by Brookfield Rheocalc software, must be carefully monitored during the tests in order to avoid external disturbances that may oscillate the spindle and affect the measurements.

The RMFs and OMFs generated have 100 Hz frequency and 31.4 kA/m intensity. Once the field is applied, a short delay is required for torque measurement stability in the absence of

any shear. Once the baseline is set, the spindle rotation speeds are fixed from the lowest value to the highest, and every set ends with a final stabilization period in order to attain the initial torque baseline. For both field types, tests are performed with the initial setting and the inverse setting on the power supplies. This modification simply changes the direction of the current circulation in the coils.

The SMF tests are performed using different magnetic field intensities, ranging from 10.4 to 36.7 kA/m. During those tests, the spindle is never allowed to rest while a magnetic field is applied in order to avoid the chance of droplets coalescence or particle agglomeration in the solutions. However, as observed by Bibette [14], no droplet coalescence is observed following the different tests because of the stabilizing effect of the surfactant, the small droplet size and the low concentration of MNPs. Apart from that, the testing procedure is identical to the one followed for the other types of magnetic fields.

For every solution, the tests with the three different field types are performed successively starting with the absence of magnetic field, and going on with RMF, OMF and finally SMF. This procedure is followed in order to minimize the impact of potential variations that could occur between different experimentation periods. The static fields are the last to be tested because they are the ones harboring the highest potential for emulsion and suspension stability disruption. During the tests, close monitoring of the coils temperature and spindle stability is required to ensure quality results. Sudden changes or inconsistencies can indicate a need for adjustment in one of the different mobile pieces of the setup or the presence of coalescence or sedimentation inside the sample.

III.4.5. Visualisation:

In order to visualize the mixing action inside the prepared emulsions, an image acquisition setup using microscopy was devised. First, a model 500 LumaScope^{TM} from Etaluma Inc. (California, USA) was disassembled and the objective was inverted to allow for its insertion inside the electromagnet bore. Then, microslides (100 µm × 1.0 mm × 50 mm slits) were filled with an emulsion sample and placed flat at the center of the magnet, under the objective. Using standard bright field settings of sample illumination *via* transmitted white light across the 100 µm slit thickness, images were collected with a 100X objective at

0.2 sec intervals with the focus plane placed 70 μm with respect to the slit upper face. The resulting images, with a field of view of 260 μm × 160 μm and a pixel size of 0.2 μm, were then strung together to create short videos demonstrating the movement inside the fluid under a rotating magnetic field and in its absence.

III.5. Results and discussion:

Figures III.3 and III.4 depict variations as a function of imposed shear rate of torque measurement results in colloidal suspensions of MNPs and in ferrofluid emulsions, respectively, with an equivalent magnetic content under the variety of different magnetic fields types and conditions. The vertical bars in Figures III.3 and III.4, representing the standard deviation on measured torques where typically repeat tests extended up to five fold, allow judging the level of scatter with respect to deterministic effects due to magnetic field properties and shear rate conditions.

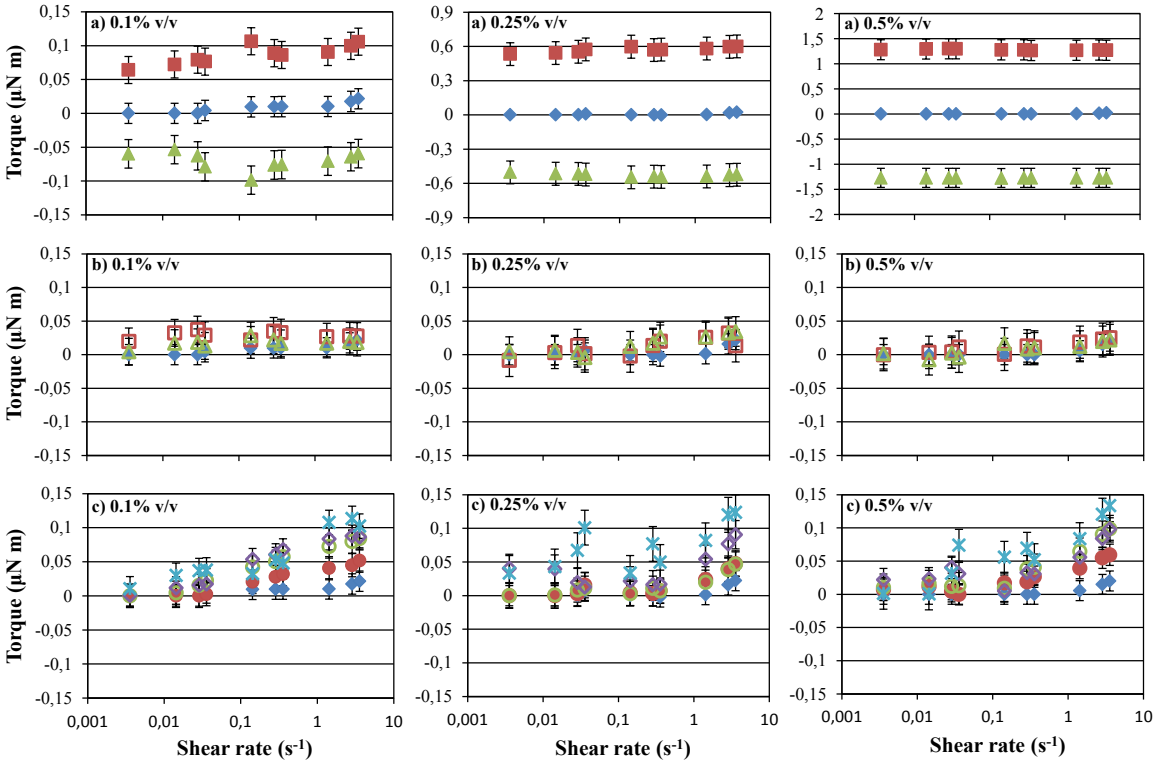

Figure III.3: Required torque to attain fixed shear rates under different magnetic fields for colloidal suspensions of magnetic nanoparticles a) RMF of 3.14 kA/m at 100 Hz; ■ = RMF in counter-rotation with spindle; ▲= RMF in co-rotation with spindle; ◆= no field; b) OMF of 3.14 kA/m at 100 Hz ; □ = initial OMF; △= inverse OMF; ◆= no field; c) ● = SMF of 10.4 kA/m; ○ = SMF of 15.7 kA/m; ◇= SMF of 26.1 kA/m; ✱=SMF of 36.7 kA/m; ◆= no field

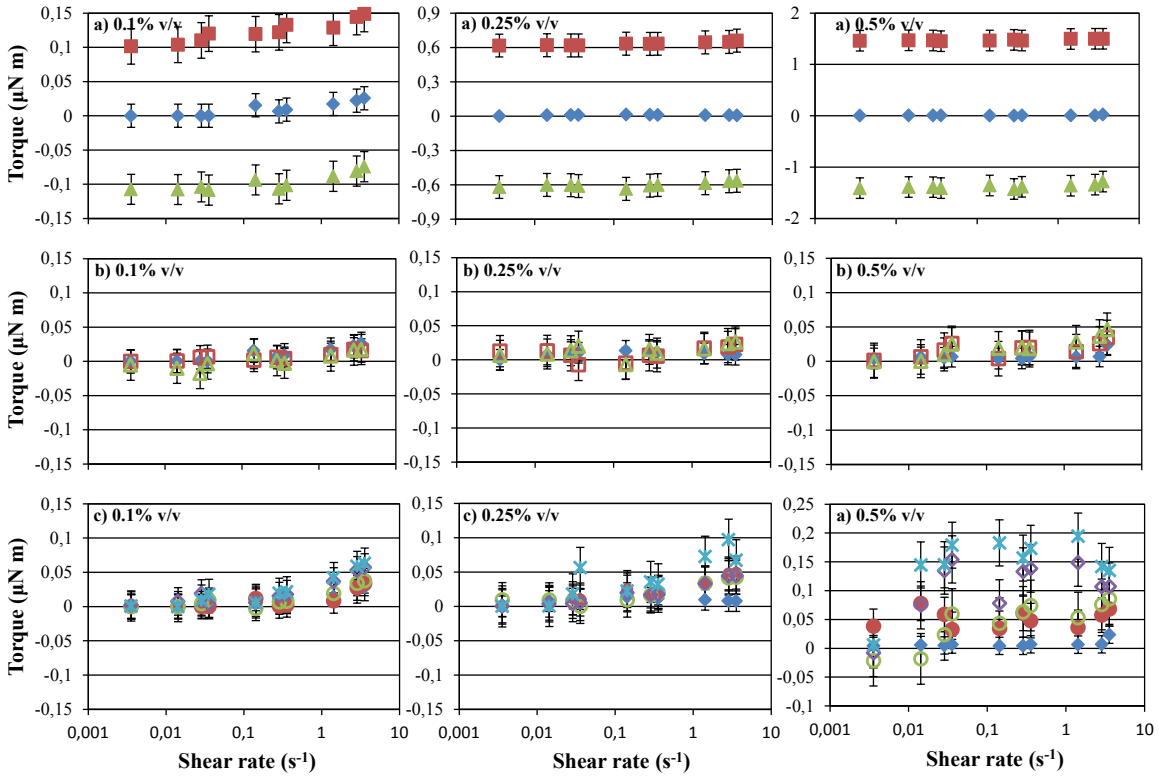

Figure III.4: Required torque to attain fixed shear rates under different magnetic fields for oil-based ferrofluid emulsions a) RMF of 3.14 kA/m at 100 Hz; ■ = RMF in counter-rotation with spindle; ▲= RMF in co-rotation with spindle; ◆= no field; b) OMF of 3.14 kA/m at 100 Hz ; □ = initial OMF; △= inverse OMF; ◆= no field; c) ● = SMF of 10.4 kA/m; ○ = SMF of 15.7 kA/m; ◇= SMF of 26.1 kA/m; ✱=SMF of 36.7 kA/m; ◆= no field

For each MNP concentration under every magnetic field, the quasi-plateaus exhibit the same amplitude and the measured torque increases with increasing the magnetic content in the liquid. More specifically, the similarities in amplitude and stability of the RMF test results indicate that the momentum of spinning MNPs inside the emulsions is successively transferred to the ferrofluid droplets containing them and then to the continuous phase of the emulsion. This fact infers that the momentum transfer at the liquid-liquid interface between the organic and aqueous phases of the emulsion occurs with an efficiency comparable to the one taking place at the solid-liquid interface in the colloidal suspensions of MNPs, resulting in an analogous effective mixing in both types of solutions. RMF results (Figures 3a, 4a) are also symmetrical for co-rotating and counter-rotating fields which is in accordance with the literature [10].

The physical interpretation put forward that the magnetic nanoparticles spinning under the effect of a *rotating* magnetic field are the cause of a cascade of events mediated by the oil droplet rotational movements which in turn convey momentum (and motion) to the continuous phase can best be appreciated from the video animation files "31042-vidIII-1" and "31042-vidIII-2" (submitted separately) acquired with the LumaScope system with the liquid-liquid magnetic emulsions placed inside transparent microslides. The videos compare 10-second image sequences acquired at 5 Hz of the same 0.10 % v/v magnetic emulsion, respectively, under RMF (f = 100 Hz, H_0 = 31.4 kA/m) and without magnetic field. When the magnetic field is off, the static character of the liquid-liquid emulsion is evident. On the contrary, enabling the rotating magnetic field led to the emergence of many eddy-like constellations of dark nodules, *ca*. 5 μm in size, representing in all likelihood *reversibly* coalesced groups of oil droplets describing coherent rotations in the enclosure thus shedding light into a specific mechanism driving mixing of the continuous phase via MNP-laden oil droplets. These movements are ascribed to a transfer of momentum between the MNPs to the surrounding droplet and then to the surrounding fluid. It will be interesting for future studies to develop rigorous mathematical formulations to describe the momentum transfer from the nanoparticles to the oil droplet to its interfacial boundary with the aqueous continuous phase ultimately to the bulk of this latter phase.

In the case of OMFs (Figures III.3b, III.4b), no significant difference is observed when comparing tests in the absence of magnetic field to the ones where it is applied. Indeed, as explained by Hajiani and Larachi [13], MNP relaxation time is sufficiently short to allow random reorientation of the magnetic dipoles in the midst of OMFs oscillating cycles, resulting in zero spatially-averaged torques when the field is reoriented and the MNPs are magnetized once again. In sum, OMFs do not bring the particles/droplets in a synchronous spin in colloidal suspension or in ferrofluid emulsion and hence they are not able to exert a measurable torque on the rotating spindle of the viscometer.

Under SMFs (Figures III.3c, III.4c), a torque increase is detected in higher magnetic content and stronger magnetic field for both types of solutions. This effect can be attributed to the MNPs magnetic moment alignment in the magnetic field direction, essentially locking them in position. From this action a resistance emerges against fluid displacements

due to MNP rigidity towards movement [13]. Consequently, the apparent viscosity increases resulting in a measured inflationary torque at each shear rate. However, the possibility of reversible droplets or formation of MNP chain-like assembly in the emulsions and suspensions when subject to SMFs for extended periods complicates the obtainment of stable measurements [14]. Such assemblies create momentarily non-uniform magnetic concentration in liquid and are able to faintly sway the spindle. Consequently, the ensuing data points get more dispersed with increasing magnetic content concentrations.

III.6. Conclusion:

In summary, the present study elicits the effects of different magnetic fields on the torque exerted by MNPs in oil-in-water ferrofluid emulsions and allows for the comparison with diluted colloidal suspensions of the same MNPs with equivalent magnetic content. Similar suspensions having previously been studied in comparable conditions by Rinaldi et al. [10] and in mixing applications by Hajiani and Larachi [13], the presented comparison permits the assertion that for an equivalent magnetic content, stable ferrofluid emulsions and colloidal MNP suspensions provide very similar effective mixing under magnetic field. With regard to RMFs, this similarity means that the momentum developed by spinning MNPs inside emulsion droplets is transferable not only to the droplets but also to the surrounding liquid medium. Based on these results, it is then possible to envision the development of versatile techniques of MNP-based microscopic mixing using ferrofluid emulsions to keep the continuous phase to be mixed completely separated from the nanostirrers.

III.7. Acknowledgments:

The authors gratefully acknowledge the Natural Sciences and Engineering Research Council of Canada and the Canada Research Chair on Sustainable Energy Processes and Materials for their financial support.

III.8. References:

[1] McTague, J. P. (2003). Magnetoviscosity of magnetic colloids. *The Journal of Chemical Physics*, 51(1), 133-136.

[2] Odenbach, S., & Thurm, S. (2002). Magnetoviscous effects in ferrofluids (pp. 185-201). Springer Berlin Heidelberg.

[3] Lu, A. H., Salabas, E. E., & Schüth, F. (2007). Magnetic nanoparticles: synthesis, protection, functionalization, and application. *Angewandte Chemie International Edition*, 46(8), 1222-1244.

[4] Zhu, Y., Stubbs, L. P., Ho, F., Liu, R., Ship, C. P., Maguire, J. A., & Hosmane, N. S. (2010). Magnetic nanocomposites: a new perspective in catalysis.*ChemCatChem*, *2*(4), 365-374.

[5] Polshettiwar, V., Luque, R., Fihri, A., Zhu, H., Bouhrara, M., & Basset, J. M. (2011). Magnetically recoverable nanocatalysts. *Chemical reviews*, *111*(5), 3036-3075.

[6] Zeng, T., Yang, L., Hudson, R., Song, G., Moores, A. R., & Li, C. J. (2010). Fe3O4 nanoparticle-supported copper (I) pybox catalyst: Magnetically recoverable catalyst for enantioselective direct-addition of terminal alkynes to imines. *Organic letters*, *13*(3), 442-445.

[7] Rosensweig, R. E. (2013). Ferrohydrodynamics. Courier Dover Publications.

[8] Odenbach, S., & Gilly, H. (1996). Taylor vortex flow of magnetic fluids under the influence of an azimuthal magnetic field. *Journal of magnetism and magnetic materials*, *152*(1), 123-128.

[9] Odenbach, S., & Störk, H. (1998). Shear dependence of field-induced contributions to the viscosity of magnetic fluids at low shear rates. *Journal of magnetism and magnetic materials*, *183*(1), 188-194.

[10] Rinaldi, C., Gutman, F., He, X., Rosenthal, A. D., & Zahn, M. (2005). Torque measurements on ferrofluid cylinders in rotating magnetic fields. *Journal of magnetism and magnetic materials*, *289*, 307-310.

[11] Soto-Aquino, D., & Rinaldi, C. (2011). Transient magnetoviscosity of dilute ferrofluids. *Journal of Magnetism and Magnetic Materials*, *323*(10), 1319-1323.

[12] Hajiani, P., & Larachi, F. (2012). Reducing Taylor dispersion in capillary laminar flows using magnetically excited nanoparticles: Nanomixing mechanism for micro/nanoscale applications. *Chemical Engineering Journal*, *203*, 492-498.

[13] Hajiani, P., & Larachi, F. (2013). Controlling lateral nanomixing and velocity profile of dilute ferrofluid capillary flows in uniform stationary, oscillating and rotating magnetic fields. *Chemical Engineering Journal*, *223*, 454-466.

[14] Bibette, J. (1993). Monodisperse ferrofluid emulsions. *Journal of magnetism and magnetic materials*, *122*(1), 37-41.

[15] Montagne, F., Mondain-Monval, O., Pichot, C., Mozzanega, H., & Elaıssari, A. (2002). Preparation and characterization of narrow sized (o/w) magnetic emulsion. *Journal of magnetism and magnetic materials*, *250*, 302-312.

[16] Becher, P. (1965). Emulsions: theory and practice. New York, USA: Reinhold Publishing Corporation

[17] Aronson, M. P. (1989). The role of free surfactant in destabilizing oil-in-water emulsions. *Langmuir*, *5*(2), 494-501.

[18] Bibette, J., Roux, D., & Nallet, F. (1990). Depletion interactions and fluid-solid equilibrium in emulsions. *Physical review letters*, *65*(19), 2470.

[19] Bibette, J. (1991). Depletion interactions and fractionated crystallization for polydisperse emulsion purification. *Journal of colloid and interface science*,*147*(2), 474-478.

[20] Chantrell, R. W., Popplewell, J., & Charles, S. (1978). Measurements of particle size distribution parameters in ferrofluids. *Magnetics, IEEE Transactions on*,*14*(5), 975-977.

Chapter IV.

Conclusion and future works

IV.1. Key contributions:

Chapter II showed for the first time image and video evidence of the behaviour at the micro-scale of a magnetic nanofluid under the action of rotating magnetic fields. The videos and images gathered allowed for a descriptive study of the coherent vortical structures emerging from the inception of nano-convective zones around each MNP in which the mixing mechanism is enhanced by particle motion. Furthermore, an innovative implementation of a 2-dimensional discrete wavelet transform based multi-resolution image textural analysis method permitted a quantitative assessment of the detected structures at different levels in the images, correlating and supporting the visual previous visual interpretations. Overall, the study showed that every investigated parameter, i.e. suspension magnetic core volume fraction, MNP size as well as magnetic field intensity, frequency and type, has a considerable effect on the emerging coherent vortical structures in the nanofluid. Increasing the magnetic core volume fraction was found to greatly intensify the size and coverage of the structures, as was the case for increasing the frequency or the intensity of the applied RMF. The size of the MNPs affected the scale and distribution of the perceptible structures, with bigger particles generating slightly smaller structures, but in a larger number and with a narrower size distribution. Finally, the sharp difference between RMF, OMF and SMF was presented, with RMF giving rise to circular vortical structures while OMF and SMF generated linear, quasi-static structures. This organisation represents well the magnetization behaviour of the individual nanoparticles in these fields.

Chapter III made the case for the use of oil-based magnetic nanofluid emulsions to initiate mixing in an aqueous phase in applications where direct contact between the MNPs or the surfactant and the continuous phase must be avoided. The concept was evaluated by establishing a comparison in the torque engendered inside the emulsions with the one engendered in equivalent colloidal aqueous MNP suspensions of equal magnetic content when both are subjected to RMFs, OMFs and SMFs. The results reveal that the mixing intensity for the two types of solution present the same amplitude that for equal magnetic content, it varies proportionally to the intensity of the applied field for the three considered field types. From these facts a deduction is made stating that the momentum stemming

from the spinning MNPs inside the emulsions is sufficient be transmitted to the organic droplets of the dispersed phase containing them and then to the aqueous continuous phase.

IV.2. Suggested future work:

In closing, the following directions for future work are suggested to extend and build upon the results presented in this work:

1. Quite recently, a colloidal suspension of MNPs (50 nm median average diameter) mixed with micromagnetic particles, or MMPs (1 μm median average diameter), was prepared and showed to be stable without significant sedimentation and agglomeration under RMF. Such a polydisperse mixture of MNPs and MMPs may be exploited to generate mixing in different length scales in suspension. Establishing an experimental framework in which multi-scale mixing can enhance distinguishable properties of a system would be an interesting development for applications involving macroporous or mesoporous materials.

2. Applying the concept of nanomixing directly to other chemical engineering systems could also help to identify its practical advantages and limitations. For example, a small packed bed reactor fabricated in order to be fed by colloidal suspensions of MNPs could bring the technology one step close to real world application. This reactor would have to be equipped with two sets of conductivity electrodes to measure tracer concentration during RTD tests. The ability of the nanomixing technique to promote and enhance mixing in pores and liquid films when subjected to RMFs would have to be closely examined as it may affect the RTD in the reactor.

3. Developing a mathematical model to test and compare the experimental results obtained from previous nanomixing experiments would also be a great tool for a better understanding of this phenomenon. The first step would be to apply the current ferrohydrodynamic formulation to predict the existing experimental results. Many observed and measured physical parameters could be determined by fitting theoretical predictions to the current measurements, like vortex viscosity, spin viscosity, ferrofluid spin velocity, and spin velocity boundary conditions. However,

since current ferrohydrodynamic theory considers magnetic nanofluids as uniform continuums in which angular momentum can be exchanged with an external magnetic field, the phenomenon of nanomixing between individual nanoparticles may not be adequately represented.

4. Closer to the present body of work, devising a particle image velocimetry (PIV) protocol to study magnetic nanofluids subjected to time-varying magnetic fields would allow much more precise and descriptive quantitative analysis of the emerging structures. A great body of literature exists to apply different wavelet based analysis to PIV measurements and the parallel and comparison of the structures arising in static magnetic nanofluids under RMF could be made with the coherent structures detected in classic fluid turbulence at the same scale.